INTERNATIONAL ATOMIC ENERGY AGENCY
UNITED NATIONS EDUCATIONAL, SCIENTIFIC AND CULTURAL ORGANIZATION

INTERNATIONAL CENTRE FOR THEORETICAL PHYSICS
34100 TRIESTE (ITALY) - P.O.B. 586 - MIRAMARE - STRADA COSTIERA 11 - TELEPHONE: 2240-1
CABLE: CENTRATOM - TELEX 460392 - I

SMR/291 - 34

SPRING COLLEGE IN CONDENSED MATTER
ON
"THE INTERACTION OF ATOMS & MOLECULES WITH SOLID SURFACES"
(25 April - 17 June 1988)

THE STRUCTURE OF MOLECULES ON SURFACES AS DETERMINED USING ELECTRON STIMULATED DESORPTION (ESD) AND PHOTON STIMULATED DESORPTION (PSD)

Theodore E. MADEY
Surface Structure and Kinetics
National Bureau of Standards
United States Department of Commerce
Gaithersburg, Maryland 20899
USA

"The Structure of Molecules on Surfaces as Determined Using Electron Stimulated Desorption (ESD) and Photon Stimulated Desorption (PSD)"

Theodore E. Madey
National Bureau of Standards
Gaithersburg, MD 20899 USA

Goal of Lectures:

a) To discuss basic physics of ESD and PSD

b) To demonstrate utility of electron stimulated desorption ion angular distributions (ESDIAD) for determining molecular structure at surfaces

c) To discuss specific examples:

* H_2O, CO, NH_3 ... on clean metals
* influence of additives (impurity atoms) on structure and reactivity
* adsorption on semiconductors
* oxide surfaces

Electron and Photon Stimulated Desorptio (ESD/PSD)

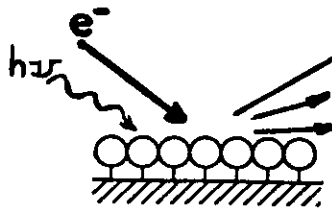

ions (+, -)
neutrals (including metastables
"cracking" of adsorbed layer

Structural information contained in Electror Stimulated Desorption Ion Angular Distribution (ESDIAD)

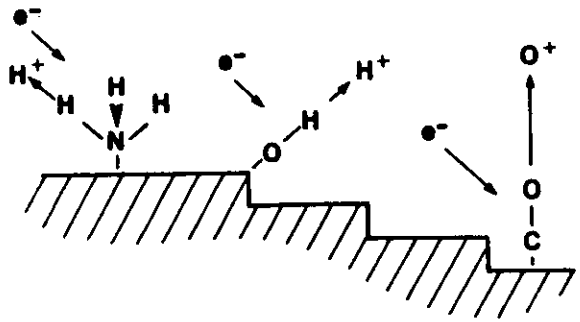

Outline of Lectures

I. Introductory remarks

II. Basic Mechanisms of ESD/PSD
- Experimental observations
- Generalized "3 step" model
- Redhead-Menzel-Gomer model (valence excitations)
- Knotek-Feibelman model (Interatomic Auger decay in maximal valency materials)
- Generalized Auger Stimulated Desorption
- Coulomb explosions
- Cross sections

III. ESDIAD
- Bond angle/ion desorption angle relation
- Experimental procedures
- Perturbations on trajectories: image effects, reneutralization

IV. Specific examples:
- A. H_2O on surfaces
- B. CO on metals
- C. NH_3 adsorption: role of impurities
- D. Adsorption on Silicon: H_2O, HF
- E. PF_3 on metals: dynamical effects
- F. Negative ion ESDIAD
- G. Beam damage in surface analysis

V. Future trends

Key References in ESD/PSD

Electron and Photon Stimulated Desorption: Probes of Structure and Bonding at Surfaces", T.E. Madey, Science 234, 316 (1986).

"Desorption Induced by Electronic Transitions - DIET-I", Springer Series in Chemical Physics 24, Eds. N.H. Tolk, M. Traum, J.C. Tully, T.E. Madey (Springer, Berlin, 1983).

"Desorption Induced by Electronic Transitions - DIET-IV", Springer Series in Surface Sciences 4, Eds. W. Brenig and D. Menzel (Springer-Verlag, Berlin, 1985).

"Experimental Methods in Electron and Photon-Stimulated Desorption", T.E. Madey and R. Stockbauer, in Methods of Experimental Physics, Vol. 22, Eds. R.L. Park and M.G. Lagally, (Academic Press, New York, 1985) p. 465.

"Desorption Induced by Electronic Transitions: Some Recent Progress", D. Menzel, Nucl. Instr. Methods B 507 (1986).

"Characterization of Surfaces Through Electron and Photon-Stimulated Desorption", T.E. Madey, D.E. Ramaker, and R. Stockbauer, Ann. Rev. Phys. Chem. 35, 215 (1984).

M.L. Knotek, Rep. Prog. Phys. 47 1499 84)
M.L. Knotek and P.J. Feibelman, Surf. Sci. 90, 78 (1979)

II. Basic Mechanisms

GENERAL EXPERIMENTAL OBSERVATIONS IN ELECTRON AND PHOTON STIMULATED DESORPTION

Some of the basic experimental observations (1–10) that characterize electron and photon stimulated desorption of surface species are as follows:

1. As indicated schematically in Figure 1a, bombardment of solid surfaces containing adsorbed layers with electron or photon beams of sufficient energy (e.g. ~10 to >1000 eV) can cause desorption of ground state neutral atomic and molecular fragments, positive and negative ions, and metastable species. In addition, dissociation or "cracking" of surface molecules and surface diffusion of adsorbed species can be induced by electron bombardment. Because of the ease of detection of ions, most ESD/PSD studies have concentrated on measurements of ion desorption.

2. Most ESD/PSD processes have cross sections that are smaller than those for electron- and photon-induced dissociation and ionization of gaseous molecules. For 100 eV electrons, typical cross sections for gas phase dissociative ionization are $\sim 10^{-16}$ cm^2. Typical cross sections for ESD of adsorbed molecules are in the range 10^{-18} to 10^{-23} cm^2. In general, cross sections for desorption of neutral species are much larger than cross sections for ions, by factors of 10–100. For ESD, an ion yield of 10^{-6} ions per incident electron is considered large.

3. Most ESD/PSD ions are atomic, with H^+, O^+, F^+, and Cl^+ the species having the highest yields. Negative ions of each of these species are also seen (11), but their yields are generally smaller than for positive ions. The dominant molecular ions observed in ESD/PSD of various adsorbed monolayers include CO^+ and OH^+. ESD/PSD of condensed multilayers often result in larger, more complex ions also [e.g. $C_nH_y^+$ from condensed C_6H_{12} (12a, b) and N_3^+ from condensed N_2 (13)]. Metastable states of CO, Li, and Na have been observed (14a–c).

4. Whereas energy thresholds for the ESD of neutral species are as low as 5 eV for CO from W, thresholds for desorption of ions are higher. Thresholds for ESD/PSD of CO^+ from W and H^+ from condensed CH_3OH are 15–20 eV, while O^+ from adsorbed CO has an onset in the range 25–30 eV. The desorption of O^+ from the surfaces of certain maximal valency metal oxides are related to core hole ionization in the metal cation, typically 25–45 eV for 3d transition metal oxides. New channels for desorption are seen to appear at energies above deep core ionization thresholds, e.g. O^+ from CO and NO above O (1s) at 530 eV. Double positive ions are also observed above core hole thresholds.

5. Ion kinetic energies are generally in the range 0–10 eV.

6. ESD/PSD cross sections are very sensitive to the mode of bonding of a molecule to the substrate surface. In general, cross sections for rupture of internal bonds in adsorbed molecules (e.g. the C–O bond in adsorbed CO bound via the C atom to the substrate, or, the H–O bond in adsorbed H_2O) are higher than cross sections for rupture of metal-atom bonds (e.g. for fractional monolayers of adsorbed H or O on a metal surface). ESD cross sections for desorption of O^+ from metal surfaces are higher for adsorption of O on step and defect sites than on atomically smooth surfaces.

7. ESD/PSD ions do not generally desorb in isotropic distributions. Rather, they desorb in discrete cones of emission, in directions determined by the orientations of the surface molecular bonds that are "ruptured" by the excitation

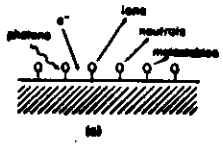

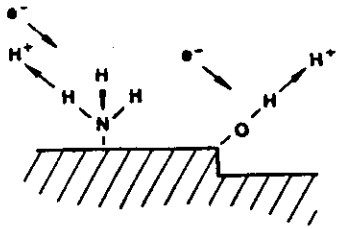

Generalized Mechanism of ESD/PSD

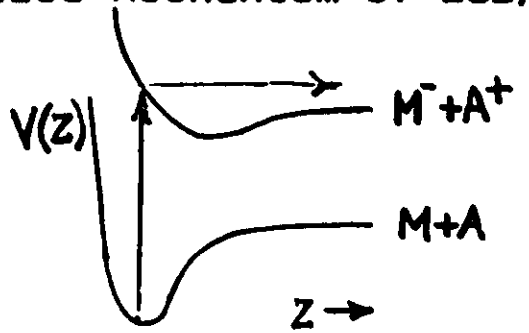

1. Fast initial excitation, ~10^{-18}s (core or valence ionization)
2. Electronic rearrangement (~10^{-15}s) to repulsive state with lifetime of 10^{-14}s
3. Modification of charge state, trajectory (image force, reneutralization)

Redhead - Menzel - Gomer Antoniewicz (7)

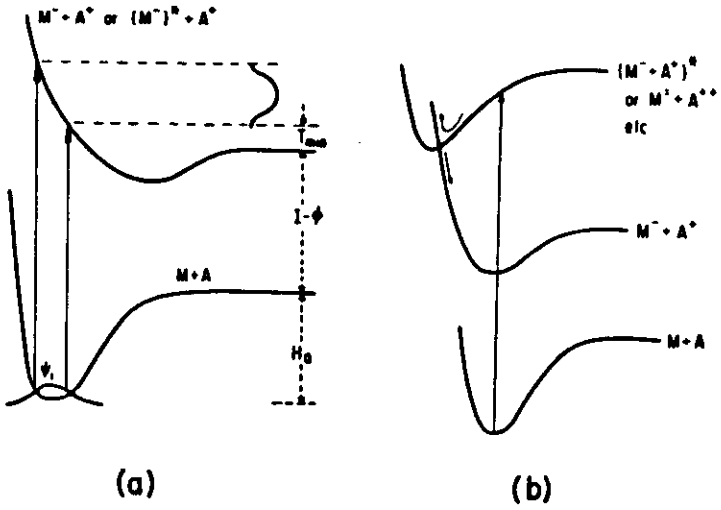

Illustration of mechanisms of ESD and PSD.

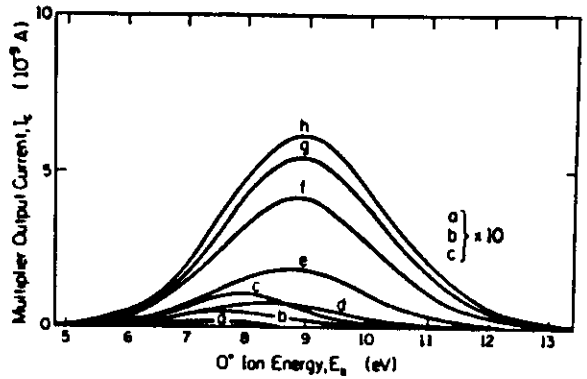

Ion Energy Distributions

FIGURE 11. Energy distributions of O^+ ions from O_2/W for various incident-electron energies V_e. Note the shift of the peak of the IED's to lower energies for bombardment energies near threshold. (From Ref. 53, with permission.) $P = 3.8 \times 10^{-10}$ Torr; $I_e = 2 \times 10^{-7}$ A; *a*, $V_e = 20$ eV; *b* = 22 eV; *c* = 24 eV; *d* = 30 eV; *e* = 40 eV; *f* = 100 eV; *g* = 200 eV; *h* = 300 eV.

Threshold Energies for ESD of neutrals, ions (8)
(Feulner et al., Phys. Rev. B 24 (1981))

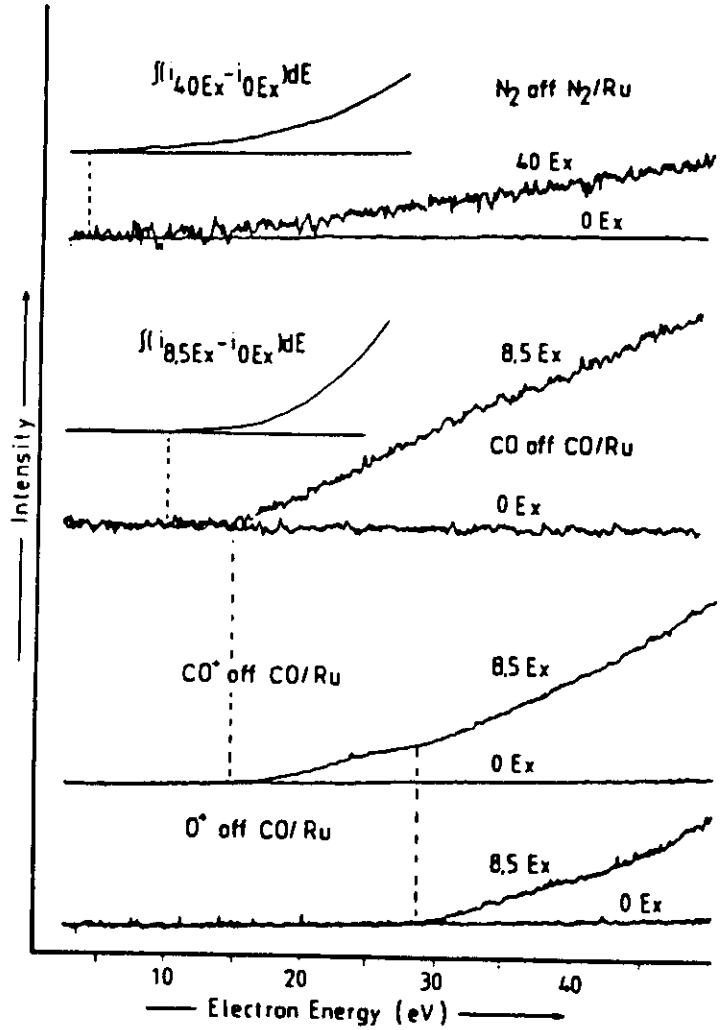

FIG. 1. Electron energy dependencies of CO, CO^+, and O^+ yields off CO/Ru(001) and of N_2 off N_2/Ru(001) in the valence region.

Mechanisms of Ion Formation: Photon Stimulated Desorption

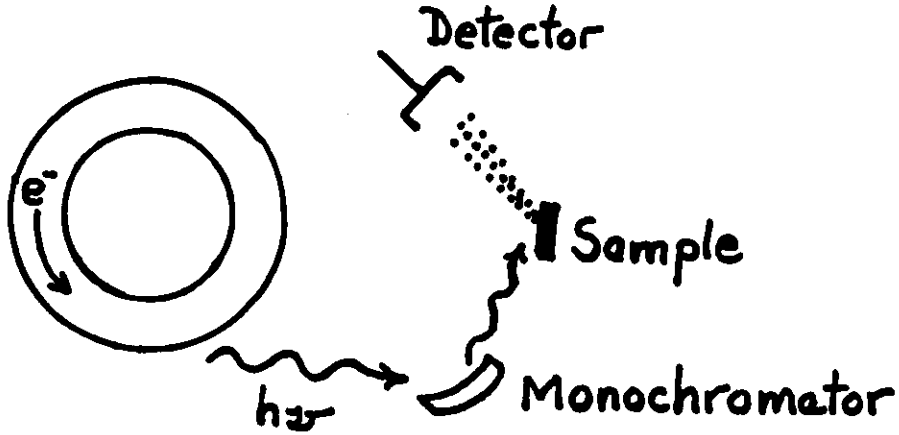

Synchrotron Radiation Facilities:
NBS SURF-II

Advantages of PSD for threshold measurements: tune radiation to break bonds selectively.

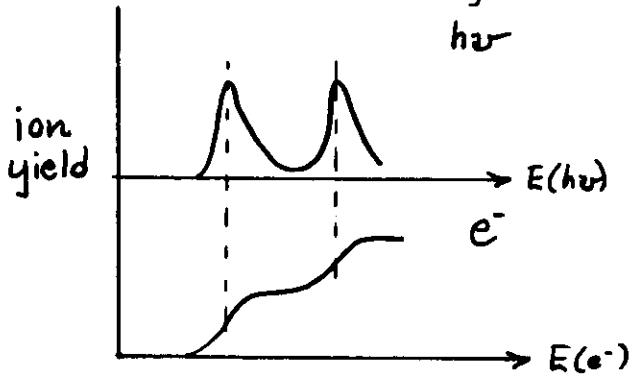

Electron and Photon Stimulated Desorpti (ESD/PSD) from TiO_2:

- desorption of O+ from a clean substrate

Knotek-Feibelman mechanism:
- ionize Ti 3p
- interatomic Auger decay
- O-- → O+

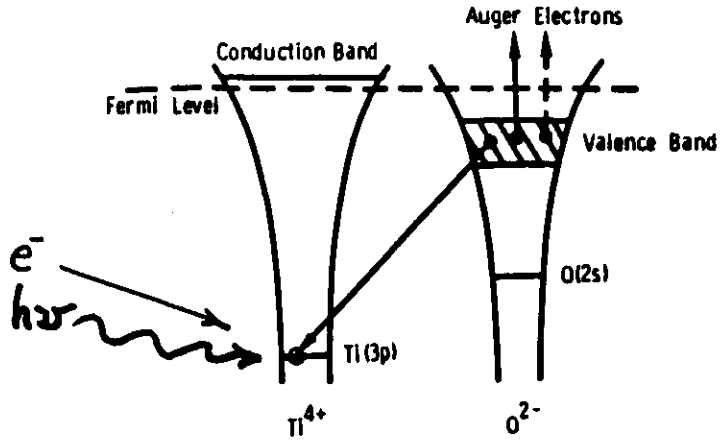

Applicable to Maximal Valency Compounds (TiO_2, WO_3, Nb_2O_5, MoO_3, etc.)

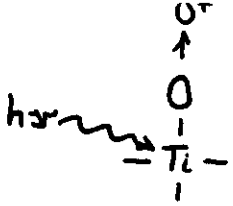

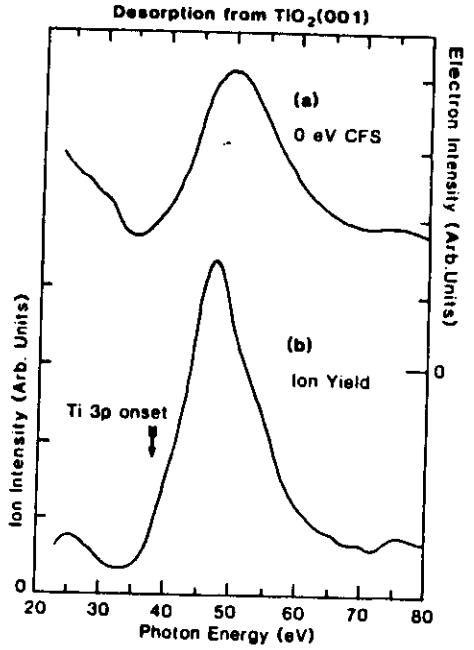

Fig. 1. Photon energy dependence of the 0 eV CFS spectrum (photoabsorption), upper curve, and the total ion yield, lower curve, from annealed TiO_2 (001)

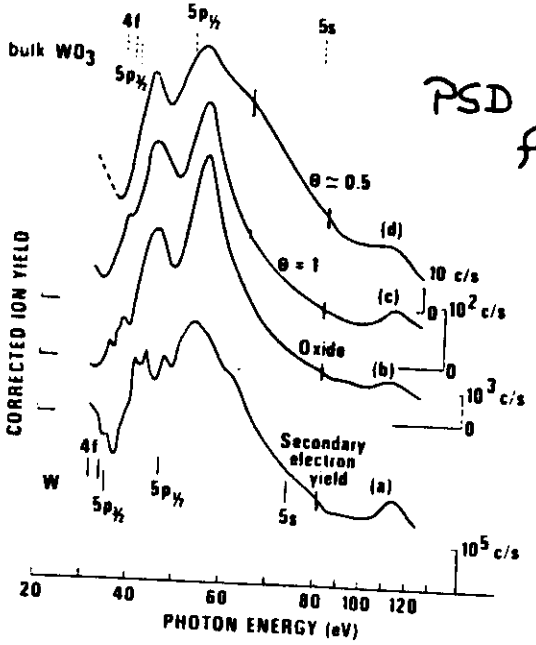

PSD of O^+ from oxygen / W(111)

Covalent Adsorbates: General Principles

(1) Desorption of singly-bonded species favored over multiply-bonded species

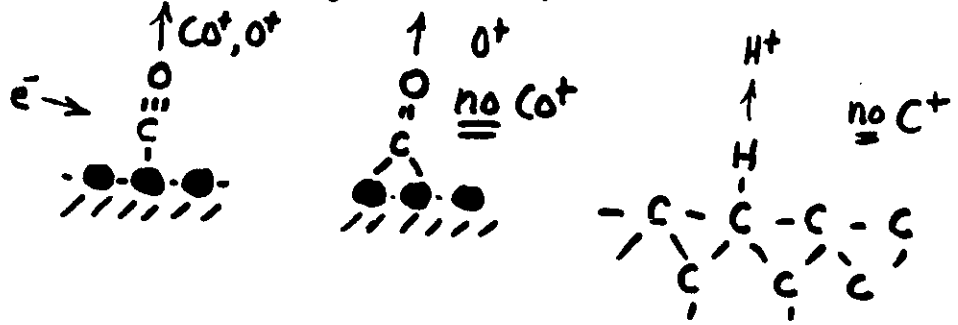

(2) "Two holes are better than one" (Feibelman)

- Geometric: orbital shrinkage
- Hubbard model: hole localization
  - two holes created on same site repel each other with energy U
  - but: kinetic energy gained by holes limited by finite bandwidth W
  - For U >> W, holes remain trapped: desorption probable!

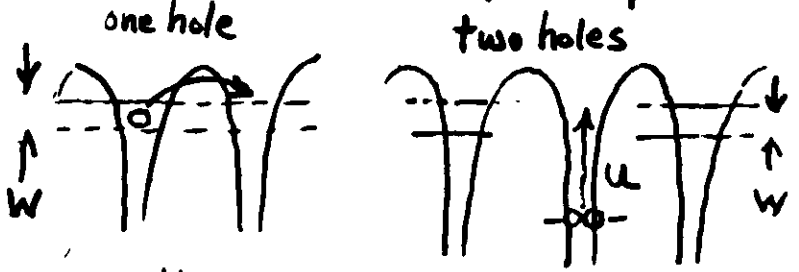

$\tau_{1h} \sim 1/W$

For $U \gg W$, $\tau_{2h} \gg 1/W$

$\sim 10^2$ larger than τ_{1h}

Auger Stimulated Desorption

(P. Feulner, D. Menzel, Phys. Rev. B24, 7427 (1981))

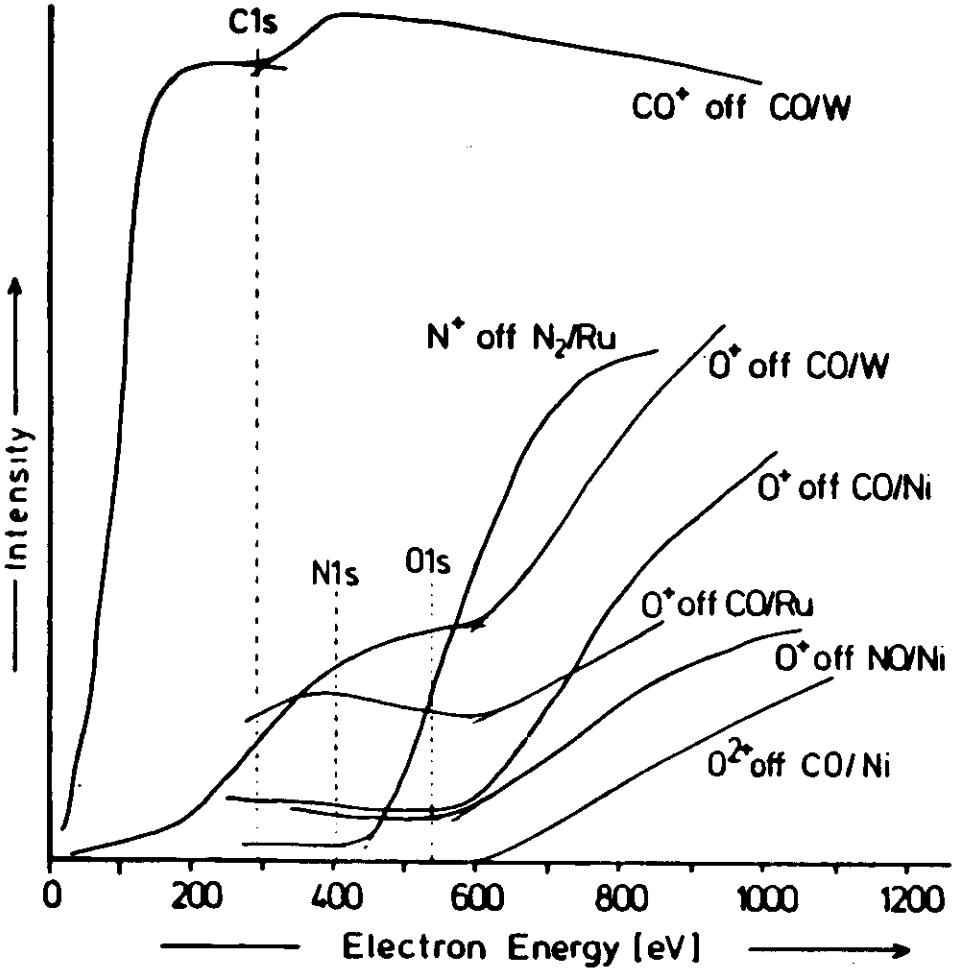

"Coulomb Explosion" Mechanism via Vacancy Cas

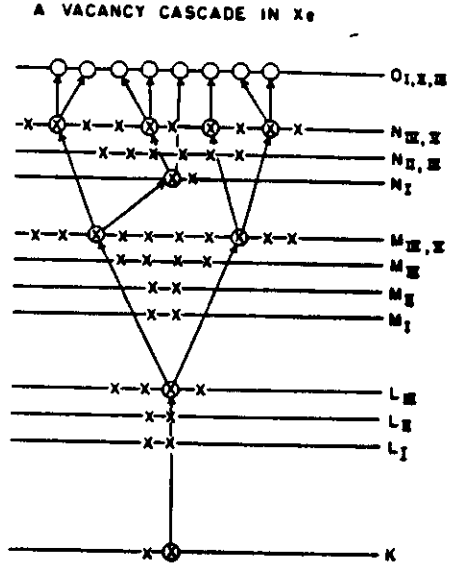

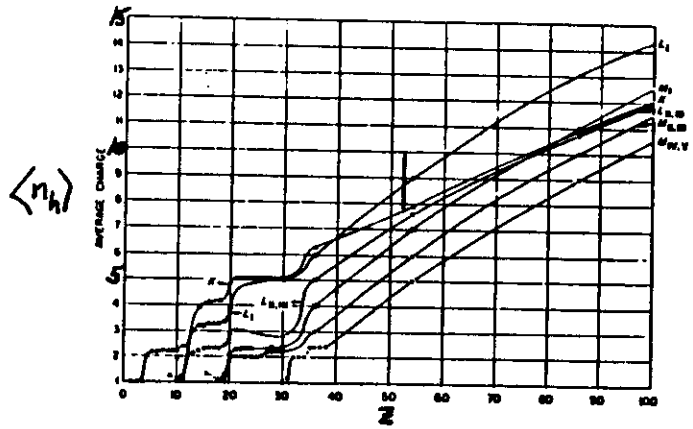

Fig. 4. Estimated average charge arising out of a sudden vacancy in the K, L and M shells as a function of the atomic number (cf. Ref. [10])

(T. A. Carlson, DIET-I Proceedings, 1983)

"Coulomb Explosion" in Molecules

$$CH_3I + \text{X-ray} \longrightarrow I^{4.7+} + C^{2+} + 3H^+ + 9.7\,e^-$$

Kinetic Energies:

I^{5+}	9eV
C^{2+}	40eV
H^+	34eV

$$Pb(CH_3)_4 + \text{X-ray} \longrightarrow Pb^{2.2+} + 3.7\,C^{1.6+} + 10.4\,H^+ + 18.7\,e^-$$

Kinetic Energies:

Pb^+	< 0.05 eV
C^+	13 eV
H^+	29 eV

Quantitative Aspects of ESD

(a) "Total" Desorption Cross Section

For electron bombardment of an adsorbed layer,

$$-\frac{dN}{dt} = nQN \qquad (1)$$

N: surface coverage (molecules/cm²)
n: electron flux (e^-/cm² s)
Q: cross section for desorption (cm²)

But $n = \frac{I_e}{A\epsilon}$ $\quad I_e$: e^- current (amps), A: beam area (cm²), $\epsilon = 1.6 \times 10^{-19}$ C

$$-\frac{dN}{dt} = \frac{I_e Q}{A\epsilon} N \qquad (2)$$

$$N(t) = N_0 \exp\left\{-\left(\frac{I_e Q}{A\epsilon}\right)t\right\} \qquad (3)$$

or $N(t) = N_0 e^{-t/\tau}$ $\quad \tau = \frac{A\epsilon}{I_e Q}$ (4)

[For $I_e = 5\mu A$, $A = 1\,mm^2$, $Q = 10^{-16}\,cm^2$, $\tau = 3$ sec!]

Measure N(t) by work function, Auger signal, thermal desorption spectroscopy, LEED, etc.
Also: direct detection of neutrals

(b) Ionic cross section

$$i^+ = I_e Q^+ N \qquad (5)$$

where i^+ = measured ion current
Q^+ = cross section for desorption of ions

To measure Q^+, we need to know N. This may be a problem, since N may be a small fraction of the total adsorbate coverage.

We can also measure Q by monitoring decay of ion current.

$$\frac{di^+}{dt} = I_e Q^+ \frac{dN}{dt} \qquad (6)$$

But from (1) above,

$$\frac{di^+}{dt} = I_e Q^+ n Q N = n Q\, i^+ \qquad (7)$$

Integrate to find

$$i^+ = i_o^+ \exp\left\{-\left(\frac{I_e Q}{A\epsilon}\right)t\right\} \qquad (8)$$

$$= i_o^+ e^{-t/\tau}$$

TABLE III. Some Representative Cross Sections for ESD of Adsorbed Species

Adsorbate	Substrate	Binding State	Ion	Ionic Cross Section Q^+ (cm²)	Electron Energy (eV)	Total Cross Section Q (cm²)	Dissociation-Desorption Ratio	Threshold (eV)	IED Peak (eV)
CO	Ir(111)	$\theta = 1/3$	—	—	86	0.8×10^{-17}–1.7×10^{-17}	≤0.01–0.02	—	—
CO	Ir(111)	$\theta = 1/3$	—	—	2500	1×10^{-17}	—	—	—
CO	Pt(111)		—	—	1500	5.4×10^{-18}	0.04	—	—
CO	W	Virgin	—	—	80	3×10^{-19}	—	—	—
		α	—	—	80	3×10^{-18}	—	—	—
		β	—	—	80	3×10^{-21}	—	—	—
CO	W	1	CO^+	1–2×10^{-20}	100	3×10^{-19}	—	15.1	1
		2	O^+	1–2×10^{-20}	100	3×10^{-18}	—	18.7	7
O_2	Te film	10 Å TeO_2	—	—	2000	3×10^{-18}	—	—	—
O_2	Ti	—	—	—	300	10^{-19}–10^{-19}	—	—	2
H_2	W(100)	$\theta \le 0.2$	H^+	2×10^{-23}	100	—	—	—	—
H_2	W	$\theta < 1$	H^+	3×10^{-23}	100	—	—	—	—
C_6H_{12}	Ru(001)	$\theta < 1$	H^+	—	150	8×10^{-17}	—	—	—
NH_3	Ni(111)	$\theta < 1$	—	—	100	1.6×10^{-16}	—	—	—
Xe	Ni, Pt	$\theta < 1$	—	—	1000–3000	1×10^{-17}	—	—	—

III. ESDIAD

Evidence for relation between bond angle and ion desorption angle:

1) Empirical basis

Structures of surface molecules which have been identified using various sensitive methods as well as ESDIAD

System	ESDIAD Ref.	Structural Assignment	Other Methods and Ref.
*CO/Ru(001)	[14]	standing-up CO	EELS [15], IR[16] ARUPS [17]
CO/Ni(111)	[18]	standing-up CO	EELS [19], ARUPS [20]
virgin-CO/ W(110)	[1,21]	standing-up CO	UPS [22]
CO/Pd(210)	[23]	inclined CO	IR [24]
NH_3/Ni(111)	[25,26]	bonded via N atom, H atoms oriented away from surface	ARUPS [27]
NO/Ni(111)	[28]	standing-up and inclined NO	EELS [29]
H_2O/Ru(001)	[30,31]	coverage and temperature dependent	EELS [32]
C_6H_{12}/Ru(001)	[33]	"chair" form of C_6H_{12} parallel to surface	EELS [34]
WO_3(111)	[36]	inclined W-O	LEED; crystallography

2) Physical basis

- hole localization mechanisms, Coulomb repulsion ⇒ desorption force directed along bond direction
- desorption lifetimes ($\sim10^{-14}$ to 10^{-15} s) << molecular rearrangement times (vibrations, rotations $\sim 10^{-12}$ to 10^{-13}

ESDIAD Apparatus

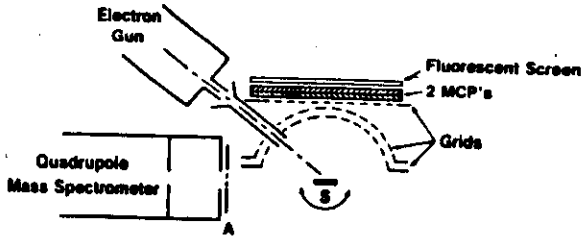

Schematic of ultrahigh vacuum ESDIAD apparatus. The sample S can be rotated. ESD ions are mass analyzed in the quadrupole mass spectrometer. ESDIAD patterns are displayed using the grid-microchannel plate (MCP)-fluorescent screen array.

Also: LEED
Auger Electron Spectroscopy
Thermal Desorption Spectroscopy
Electron Energy loss spectroscopy

Video ESDIAD$^{+,-}$ Apparatus

lsers used
- time-of-flight
easuremonts

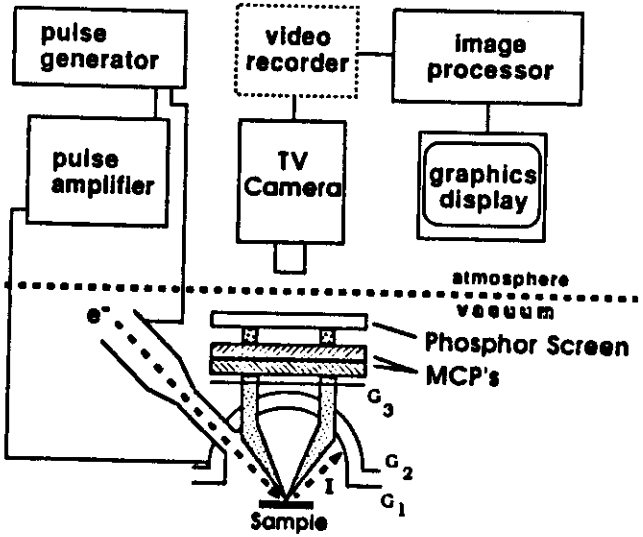

Dynamical Effects

n ESDIAD,

ion beam direction determined by orientation of molecular axis,

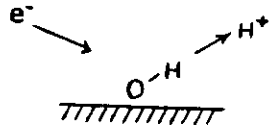

ion beam width determined by vibrational amplitude (bending, rotation)

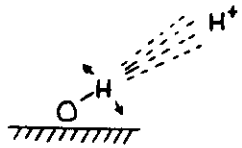

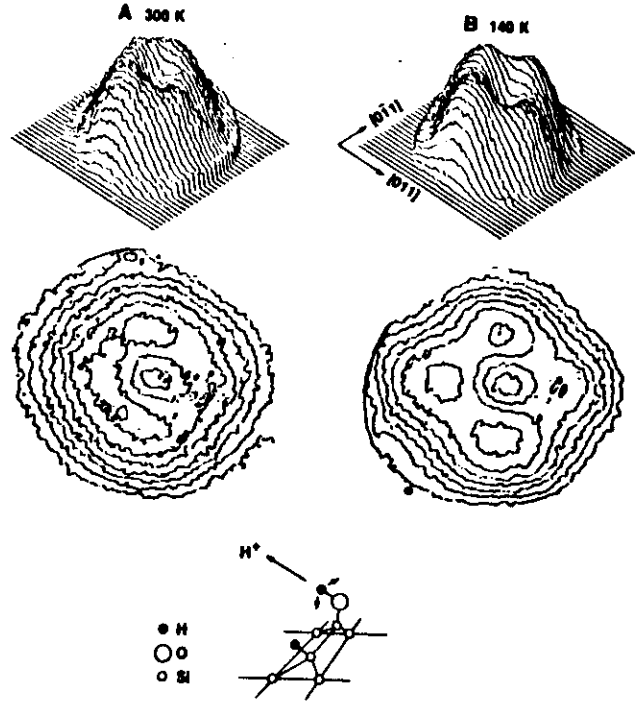

Fig. 4. H^+ ESDIAD and schematic models illustrating the bonding of OH to a Si(100) surface (*33*). (A) H^+ ESDIAD (perspective and contour plots) at 300 K; (B) H^+ ESDIAD at 140 K. A schematic bonding model in which H and OH are bound to both ends of a Si(100) dimer (*32*) is shown at the bottom. The four H^+ beams in (B) are due to ESD from degenerate dimer configurations. The decrease in resolution of ESDIAD at 300 K is due to increased vibrational motion of the OH species.

Perturbations on Ion Trajectories

(a) Image force

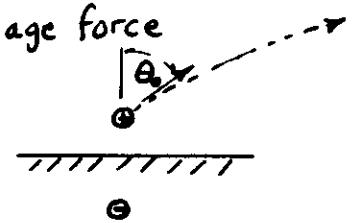

The present calculations treat the repulsive potential as an infinitely-steep repulsion acting upon the ion at a position s_0, where s_0 is the distance of the ion from the surface image plane at the instant the ion is formed (i.e., it is related to the ground state equilibrium separation of the adatom from the surface). For large ion–surface separations $s \gg s_0$, the ion moves in the attractive screened image potential $V_I(s)$, approximated by [11]

$$V_I(s) = -e^2/4(s + k^{-1}). \tag{1}$$

Here k^{-1} is the Fermi–Thomas screening length. Since the potential $V_I(s)$ is long range compared with the repulsive potential, eq. (1) is valid for all $s > s_0$. For simplicity, we assume that an ion, formed at s_0, has initial kinetic energy E_0 and moves classically in the image potential only. However, it should be noted that E_0 is a fictitious quantity since the detailed shape of the repulsive potential is unknown. A better-defined quantity is E, the final experimentally-measured ion kinetic energy at large distance from the surface

$$E = E_0 - |V_I|, \tag{2}$$

with

$$V_I = -e^2/4(s_0 + k^{-1}), \tag{3}$$

the image potential at the initial ion–surface separation s_0. Note that V_I (i.e., s_0) is not uniquely defined, but can be estimated by using Gadzuk's procedure

In this section, we derive a classical equation for the trajectory of a low energy ion leaving a metal surface under the influence of the image potential, to extend the previous results of Clinton [1] and Madey [2]. These authors followed an ion formed at the distance s_0 from the surface, with initial kinetic energy E_0 and initial desorption polar angle θ_0 measured with respect to the surface normal. They concluded, from momentum and energy conservation laws, that at large distances from the surface, the (measurable) desorption polar angle θ is given by

$$\cos\theta = \cos\theta_0 \left(\frac{1 + V_I/E_0 \cos^2\theta_0}{1 + V_I/E_0} \right)^{1/2}, \tag{4}$$

with V_I defined by eq. (3). Furthermore, if $\cos^2\theta < |V_I|/E_0$, there is no solution of (4) and hence no desorption. Thus, the condition for desorption is

$$\theta_0 \leq \theta_c = \arccos\sqrt{|V_I|/E_0}. \tag{5}$$

Recapture if $\frac{p_\perp^2}{2m} < |V_I|$

"Impulsive" model

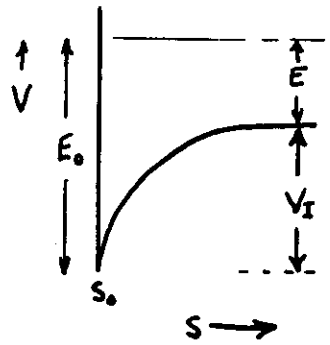

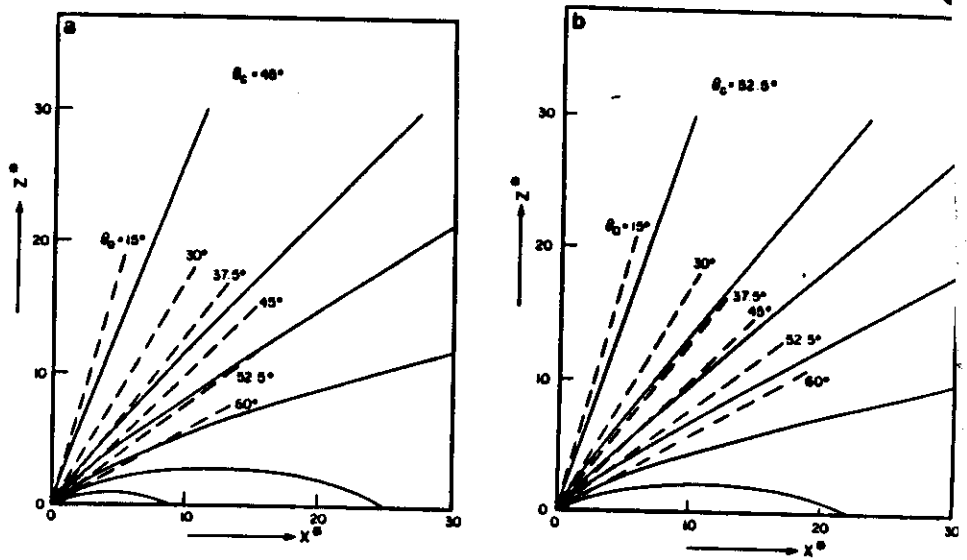

Fig. 2. Trajectories of desorbing and trapped ions in the image potential.

The main conclusions of this work can be summarized as follows:

(1) The image potential invariably causes an increase in the polar desorption angle θ of an ion leaving a planar metal surface; the image potential does not influence the azimuthal angle ϕ. The amount of distortion of the ion trajectory by the image potential is directly related to the parameter $|V_I|/E_0$ which defines the "strength" of the image potential. (V_I is the ion potential at the initial ion-surface separation, and E_0 is the initial kinetic energy.) Larger values of $|V_I|/E_0$ lead to large distortion of the trajectories.

(2) For monoenergetic, monodirectional ions there is a critical angle for desorption θ_c, which depends on $|V_I|/E_0$. For initial desorption polar angles $\theta_0 > \theta_c$, the image potential will bend the ions back to the surface, and escape is impossible. For $\theta_0 = \theta_c$, the polar angle of the final trajectory is $\theta = 90°$, parallel to the surface.

(3) For ions desorbing with a range of energies and angles (i.e., with finite energy width E_w and angular width θ_w), the results are more complex.

(a) For $\bar{\theta}_0 > \theta_c$, i.e., when the initial bond polar angle is greater than the cut-off angle, a sharp cut-off of the resultant angular distribution does not occur at $\theta = 90°$. Rather, the angular distribution is peaked at θ_p less than 90°, and the ion intensity at 90° is very low. Experimental evidence for this phenomenon has been seen in ESDIAD of H^+ from NH_3 on Ni(111) [2,18,19].

(b) The FWHM and the peak position θ_p which characterize the final angular distribution are *not* unique functions of the strength of the image potential, $|V_I|/E_0$. The ambiguity is most apparent for large values of $|V_I|/E_0$, and for large values of initial polar bond angle $\bar{\theta}_0$.

The latter conclusion means that the original surface bond polar angle $\bar{\theta}_0$ and the angular with ϕ_w for ion desorption from an adsorbed molecule cannot always be determined unambiguously from the experimental ESDIAD measurements.

Mišković, Vukanić, Madey: Surface Sci. 141, 285 (1984); 169, 405 (1986)

b) Reneutralization

Assumptions:

We adopt here the Hagstrum non-local type of reneutralization, i.e. we assume that the electron which participates in the hopping process is delocalized within the substrate conduction band. This model implies that the reneutralization rate R depends only on the ion–surface separation z, and this dependence is usually modelled by

$$R(z) = A\,e^{-az}. \tag{2}$$

One can see that this model of reneutralization affects only the polar angle dependence of ESDIAD; the azimuthal dependence is unaffected.

The ion survival probability P, i.e. the probability that the ion desorbs without reneutralization is given by

$$P = \exp\left[-\int_0^\infty R(z(t))\,dt\right], \tag{3}$$

where $z(t)$ is the time-dependent ion–surface separation in the classical trajectory approach.

It is reasonable to assume that ion desorption is caused mainly by a strong repulsive central force [2.4.11] acting between the ion and a surface atom. The repulsive potential is of the Born–Mayer type

$$V(r) = B\,e^{-br}, \tag{4}$$

where r is the distance between the ion and a surface atom.

4. Conclusions

The plots of figs. 1 and 2 are based on a limited range of parameters appropriate to one system, ESD of oxygen on W. However, the results of our calculations support the view that quantitative conclusions of bond angles based on ESDIAD measurements alone depend strongly on the measured value of polar angle θ_p. *In general*, for values of θ_p less than 30°–40° or so, one can determine the initial desorption angle, consistent with the assumptions of the simple models. For measured angles much greater than 50°, it is difficult and in most cases impossible to determine quantitatively the initial desorption angle. It was found earlier [6] that the peak angle and width of an ESDIAD beam can be insensitive to the strength of the image potential at large values of θ, and the reneutralization effects illustrated above in figs. 1 and 2 introduce further complications, as do the presence of steps, defects and other surface topographical effects. We conclude that at *large* values of θ_p, the main utility of ESDIAD is qualitative, i.e., to identify that the CBD is strongly inclined with respect to the surface normal.

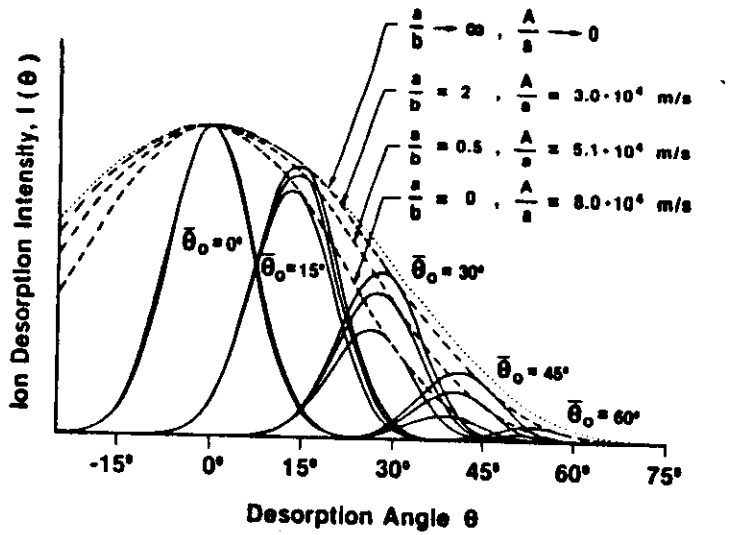

Fig. 1. Calculated effects of reneutralization on electron stimulated desorption ion angular distribution (ESDIAD) using parameters appropriate for ESD of O^+ from oxygen on tungsten. The dashed lines show the angular dependence of the survival probability P for different values of a/b, assuming isotropic initial ion angular distributions. The set of solid curves for various chemical bond directions $\bar{\theta}_0$ and various a/b is enveloped by the corresponding curve for P. The dotted curve represents the angular dependence of P for $a/b \to \infty$.

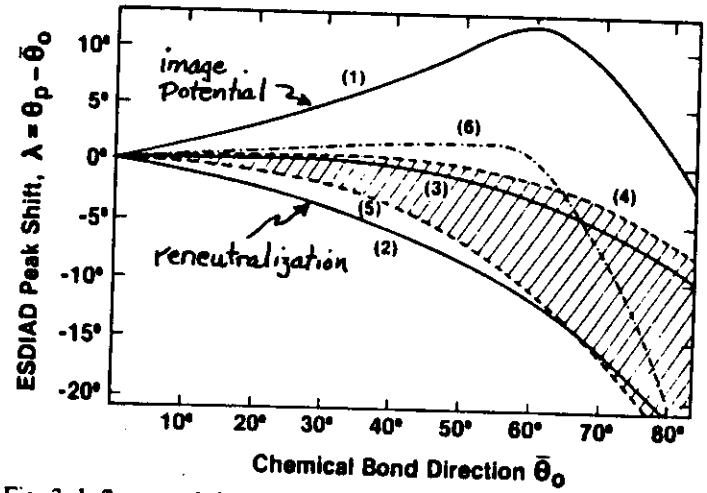

Fig. 2. Influence of the image potential (curve 1) and reneutralization processes (curve 2) on the shift of the ESDIAD peak, $\lambda = \theta_p - \bar{\theta}_0$, as a function of $\bar{\theta}_0$. The peak shift λ is defined as the difference between the measured peak position θ_p and the ground state chemical bond direction $\bar{\theta}_0$, i.e., $\lambda = \theta_p - \bar{\theta}_0$. Curve (3) is the resultant shift with reneutralization and image interaction effects calculated simultaneously for $\delta = 0.2$. The shaded area represents the region of the resultant peak shifts when δ varies from 0 (curve 4) to infinity (curve 5). Curve (6) is the sum of the curves (1) and (2).

Summary

- ESDIAD provides direct information about surface structure.

- ESDIAD sensitive to orientation of H- ligands; LEED not useful.

- ESDIAD sensitive to local bonding geometry; long range order not necessary.

IV. Specific Examples

"The Interaction of Water with Surfaces: Basic Aspects"

Unique features of adsorbed H_2O: large dipole moment, strong attractive interactions

$\mu = 1.83$ D 

- "tetrahedral" molecule
- 2 lone pair orbitals

On a surface:

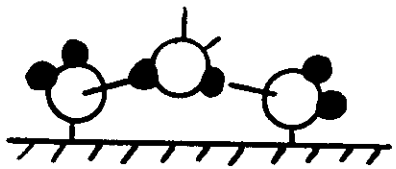

- bond via O
- H-bonding interactions
- tendency to cluster

In contrast, isoelectronic NH_3:

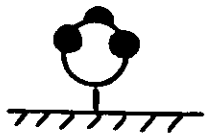

- large dipole moment
- one lone pair orbital
- repulsive lateral interactions

Outline

I. Clean Metal Surfaces

- A. - Molecular vs. Dissociative
  - Strength of H_2O Adsorption Bond
  - Theory
- B. - Structure of H_2O on Metals
  - Long Range Order and Local (Azimuthal) Order
  - Examples: H_2O on Ni(110): Dimers
    H_2O on Ru(001)

II. Additive-Dosed Surfaces

- Influence of O, Br on Order
- Hydrogen Abstraction: OH
- Dissociation Induced by K

III. Oxides

- TiO_2
- High T_c Superconductors

Dissociative vs. Molecular Adsorption of H_2O

Thermochemical Predictions:

IV B	V B	VI B	VII B	VIII B			I B	II B
22 Ti	23 V	24 Cr	25 Mn	26 Fe	27 Co	28 Ni	29 Cu	30 Zn
40 Zr	41 Nb	42 Mo	43 Tc	44 Ru	45 Rh	46 Pd	47 Ag	48 Cd
72 Hf	73 Ta	74 W	75 Re	76 Os	77 Ir	78 Pt	79 Au	80 Hg

// Dissociative // Borderline ⁘ Molecular

Experimental Observations:

IV B	V B	VI B	VII B	VIII B			I B	II B
22 Ti	23 V	24 Cr	25 Mn	26 Fe	27 Co	28 Ni	29 Cu	30 Zn
40 Zr	41 Nb	42 Mo	43 Tc	44 Ru	45 Rh	46 Pd	47 Ag	48 Cd
72 Hf	73 Ta	74 W	75 Re	76 Os	77 Ir	78 Pt	79 Au	80 Hg

// Crystal face-dependent

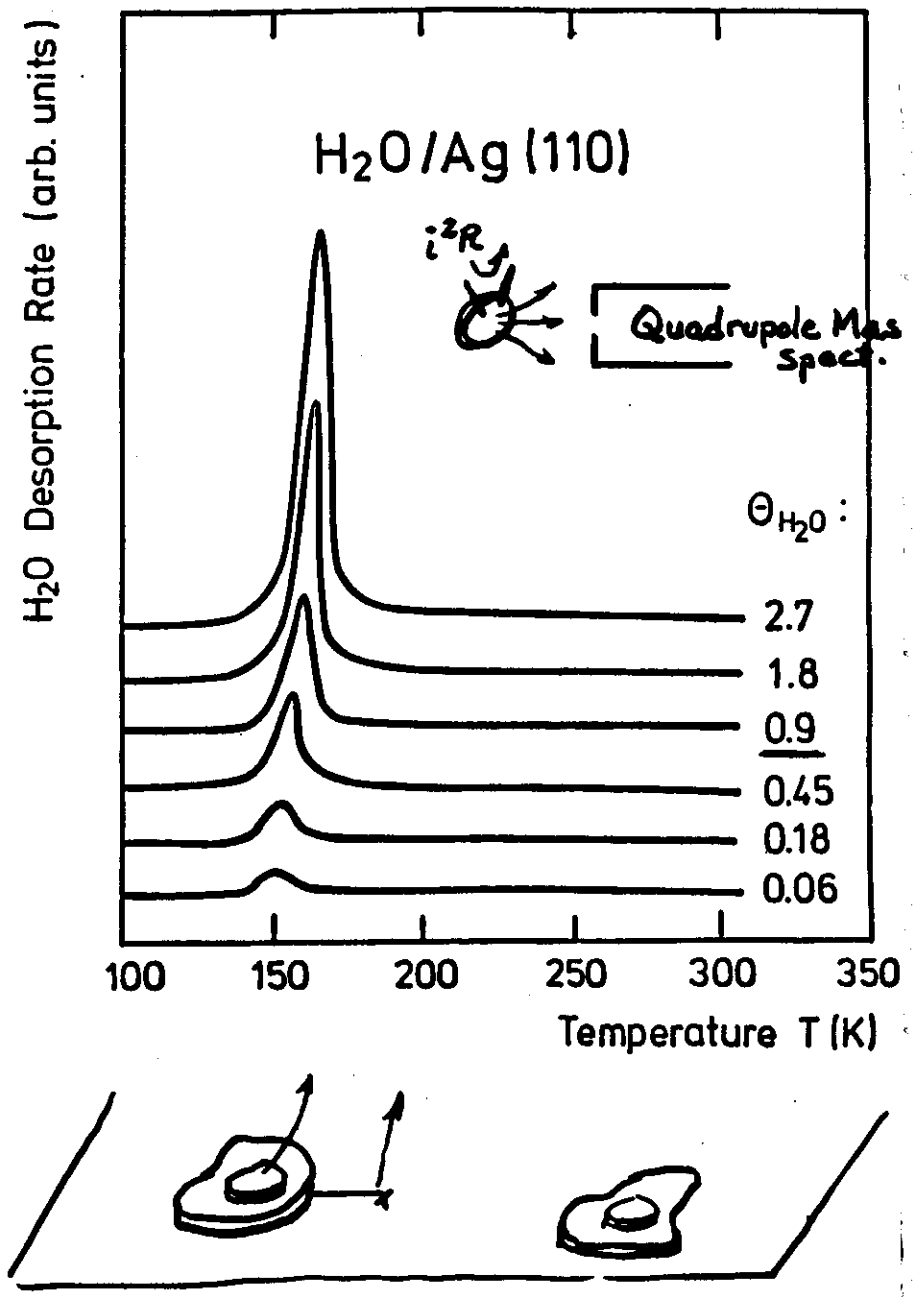

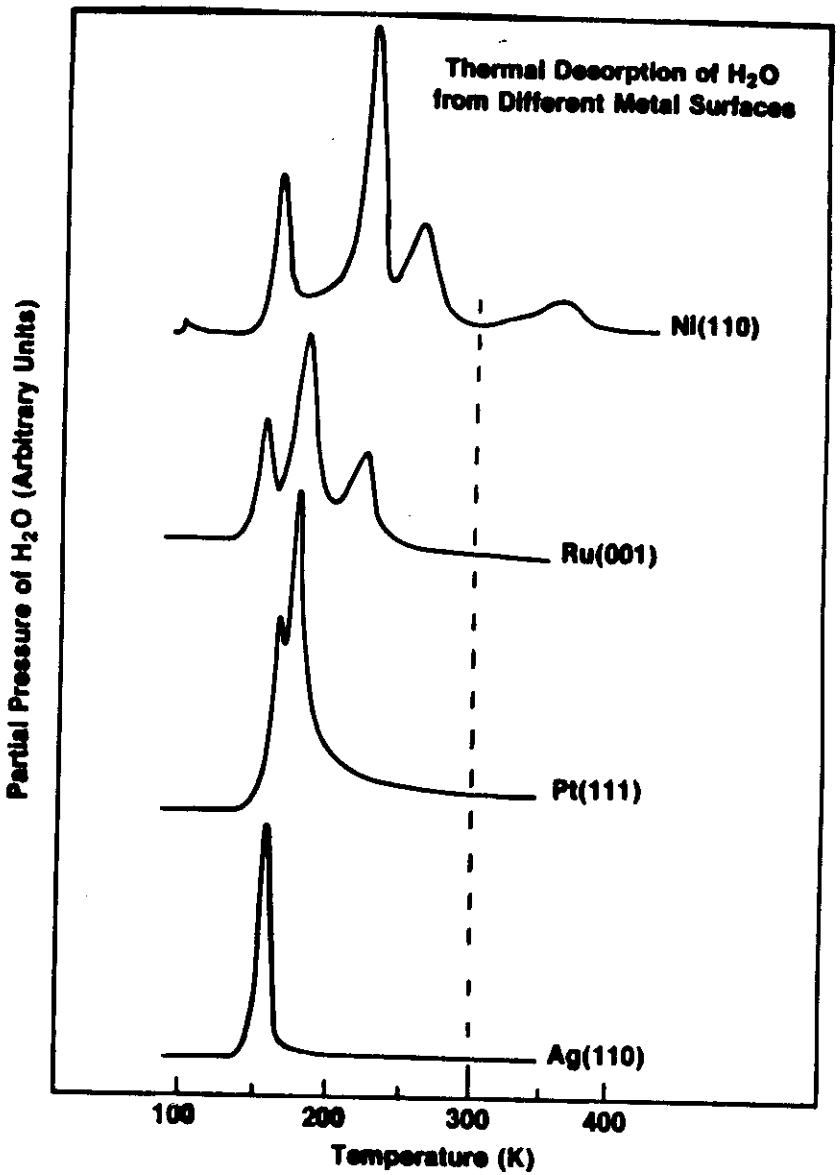

$T \leq 275\,K$ desorption of H_2O

$T \geq 275\,K$ $2\ OH \rightarrow H_2O(g) + O(a)$

Electron Density Contours for Bonding Orbitals of H_2O-Cu_5

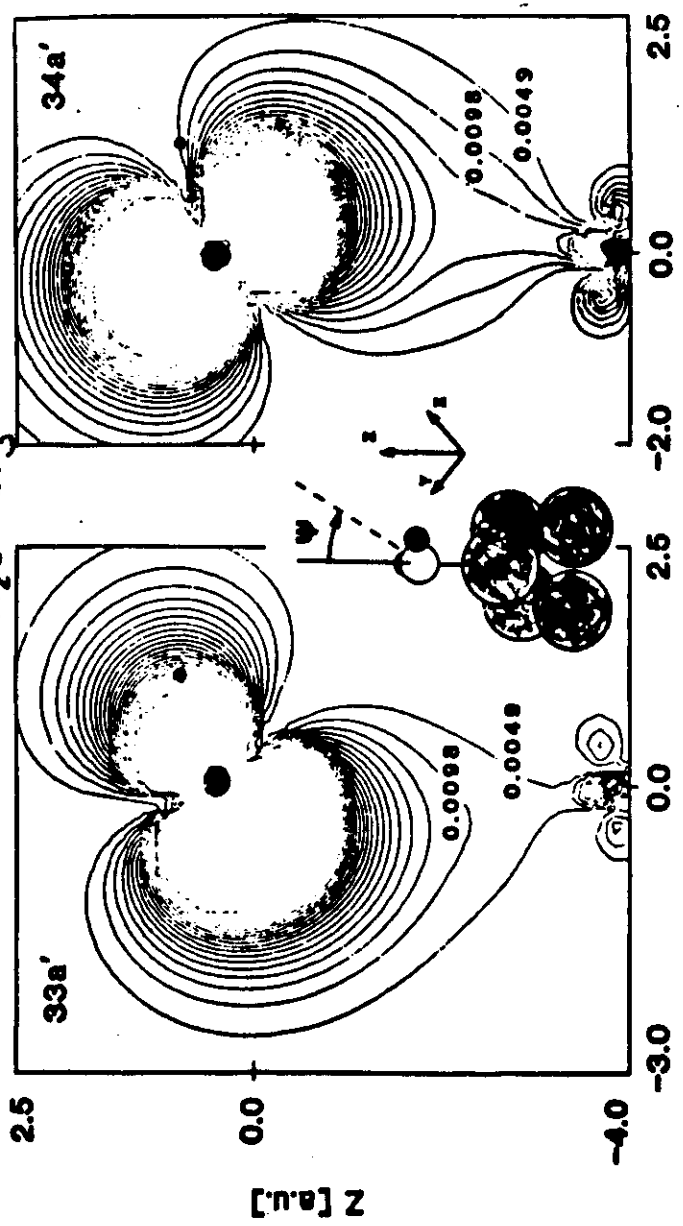

(Ribarsky, Luedtke, Landman)

Long range order (LEED):

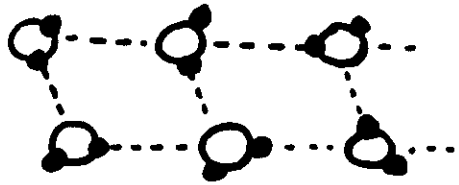

Short range, local order (ESDIAD):

- molecular orientation on surface related to substrate symmetry

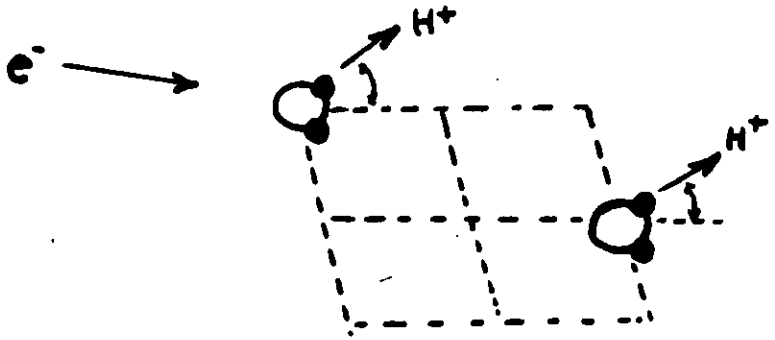

- azimuthal bond angles and/or polar bond angles the same for majority of molecules

The smallest cluster: the water dimer o

Ni, Cu(110)

Schematic ESDIAD

Model for H_2O Dimer

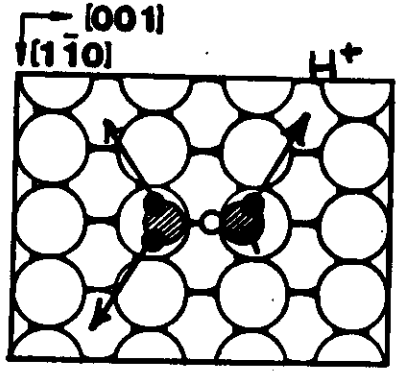

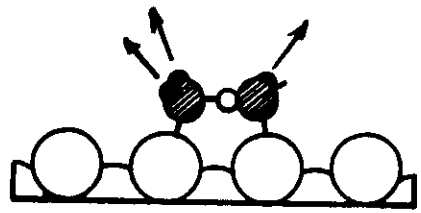

ESD - active ●

ESD - inactive ○

[001]
[1$\bar{1}$0]

Dimers

A)

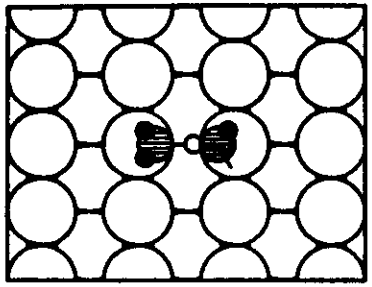

H$^+$ ESDIAD Patterns

Bilayer

B)

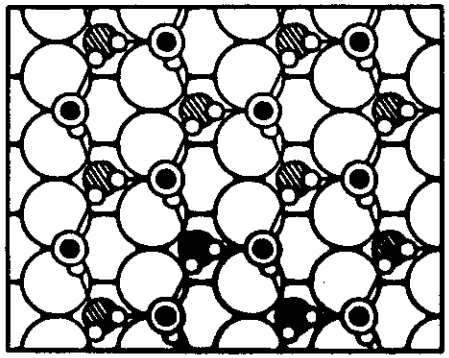

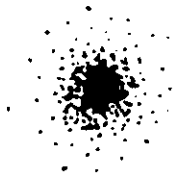

First Layer H_2O

Second Layer H_2O

ESD Active Hydrogen

ESD Inactive Hydrogen

Angle Resolved UPS (He I)

H_2O on Ni(110): evidence for dimers

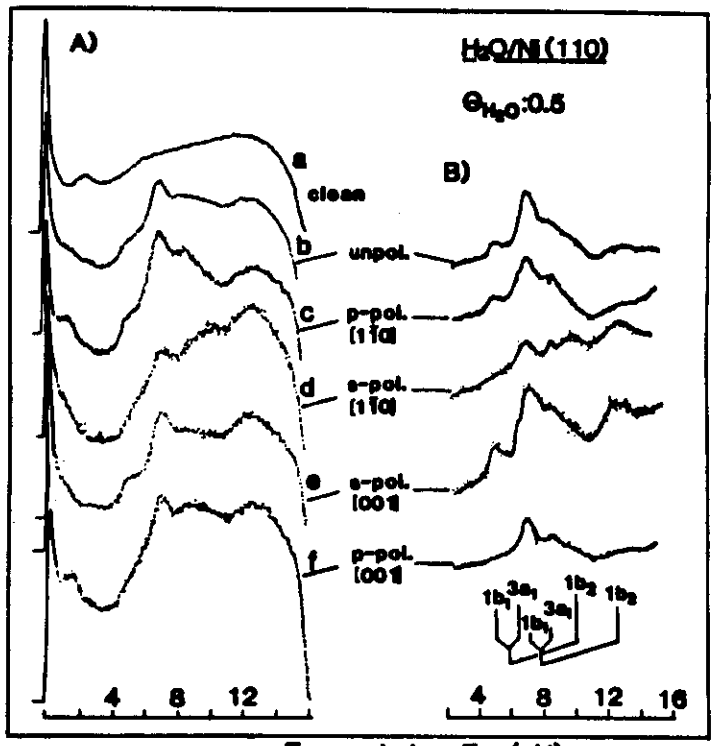

- H_2O monomers, hydrogen-bonded clusters give 3 UPS peaks: $1b_1$, $3a_1$, $1b_2$
- H_2O dimers give 6 UPS peaks

Hexagonal Clusters on Ru(0001), Re(0001)

Schematic ESDIAD:

Model for Bilayer Cluster:

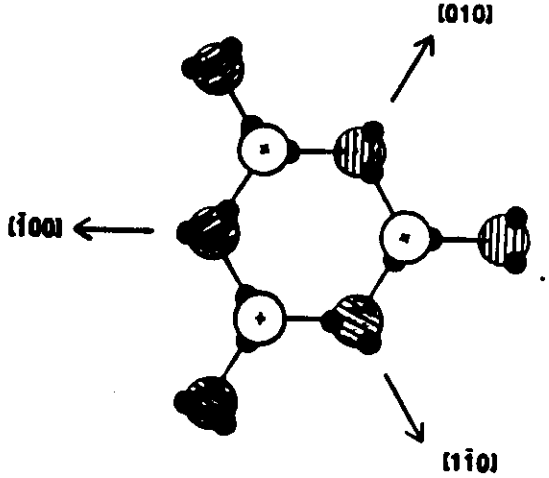

Influence of additives on surface structur

In gas phase,

What happens on surface?

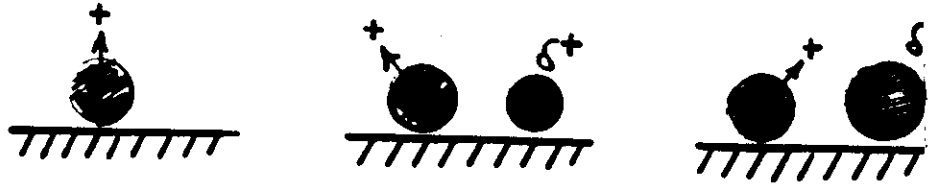

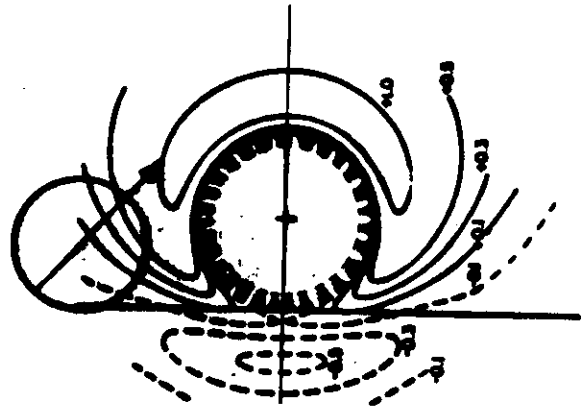

Theory (Lang, Norskov, Holloway)

(b) Model for Orientation of H_2O

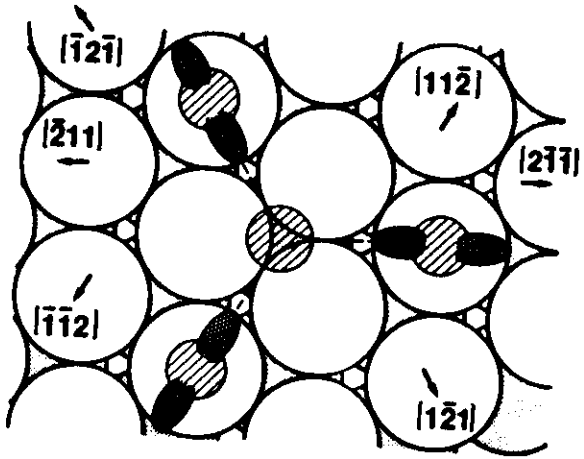

Schematic
H^+ ESDIAD

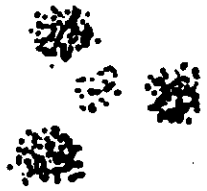

H^+ ESDIAD: Influence of Br on the Structure and Chemistry of H_2O on Ag (110)

(a) H_2O/Ag (110)

(b) H_2O + Br

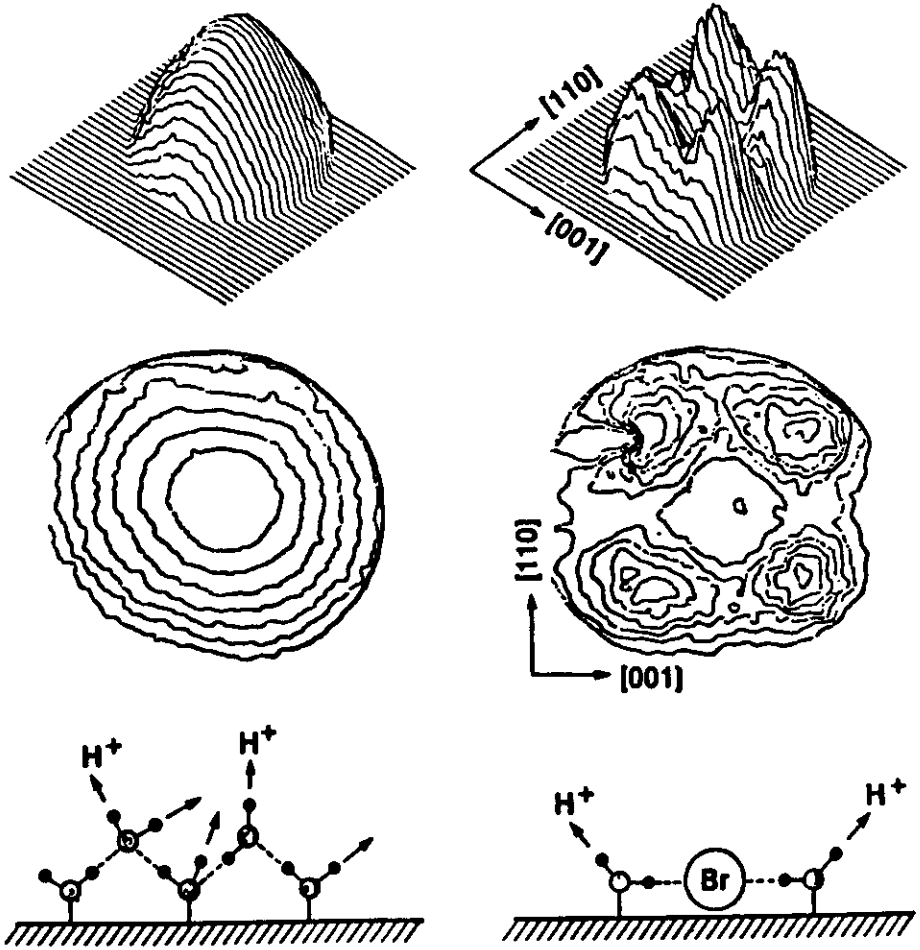

Hydrogen abstraction

$H_2O(a) + O(a) \rightarrow 2\,OH(a)$

What is the structure of OH(a)?

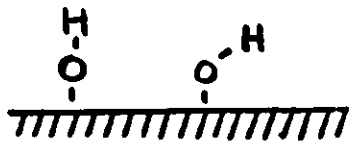

H^+ ESDIAD: Influence of O on the Structure and Chemistry of H_2O on Ag (110)

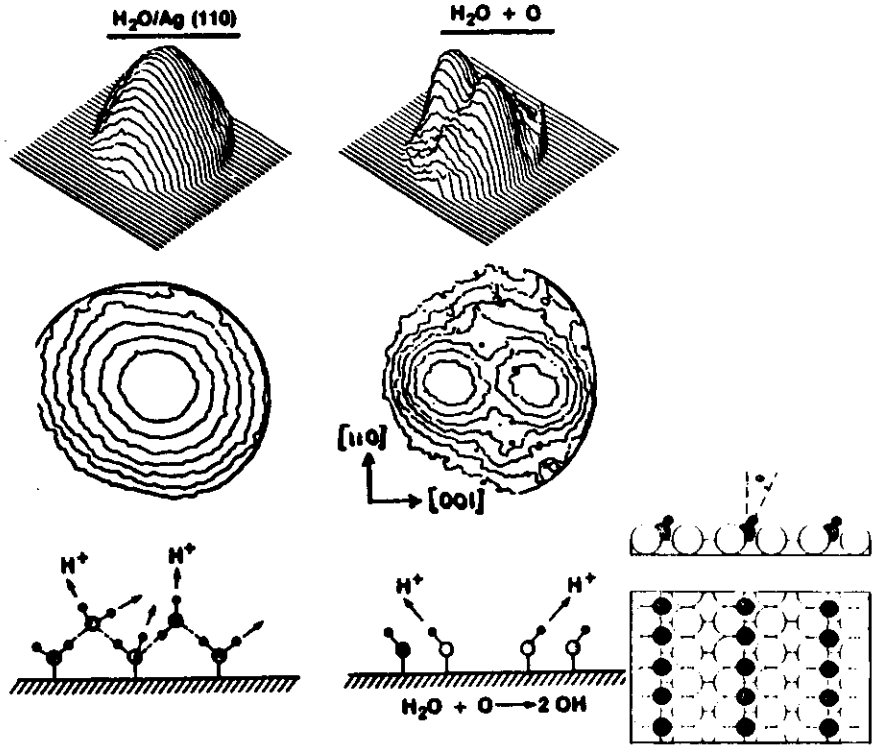

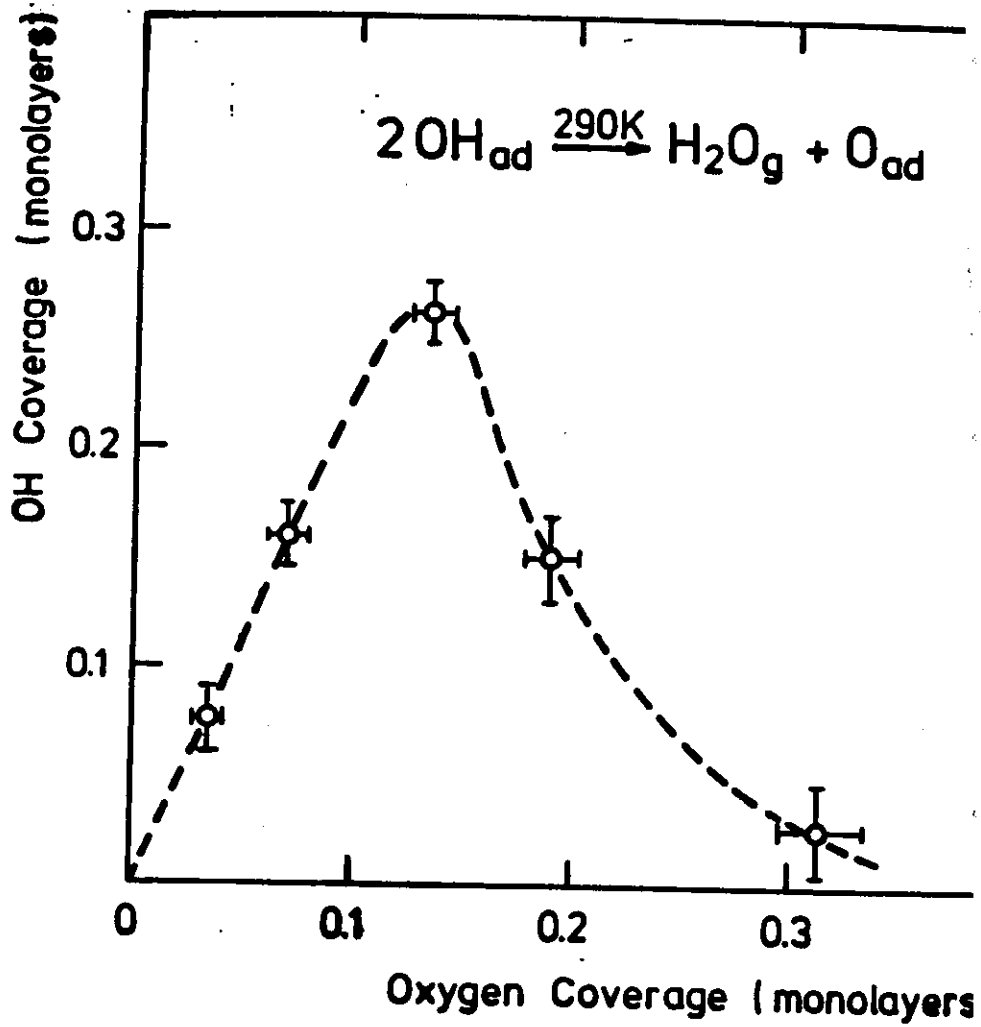

Similar data: Cu(110)
Ag(110)
Ni(110)
Pd(100)

Dissociation of H_2O on K-dosed Pt(111)

(Kiskinova, Pirug, Bonzel)

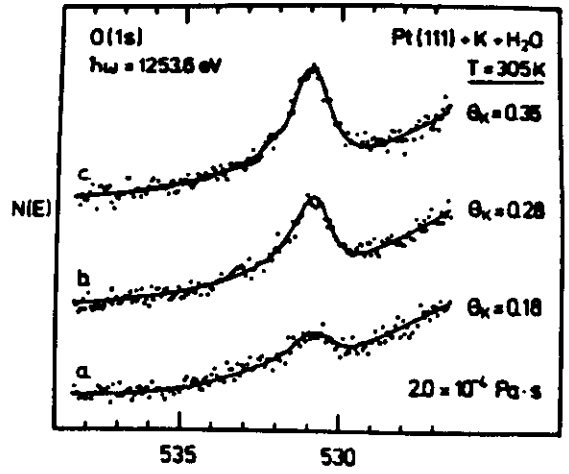

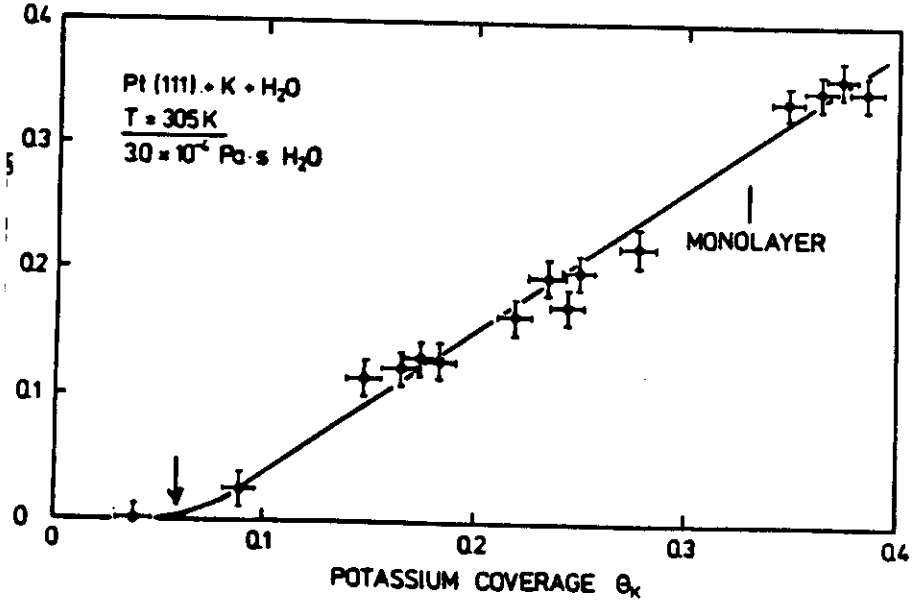

Interaction of H_2O with TiO_2

T = 300K

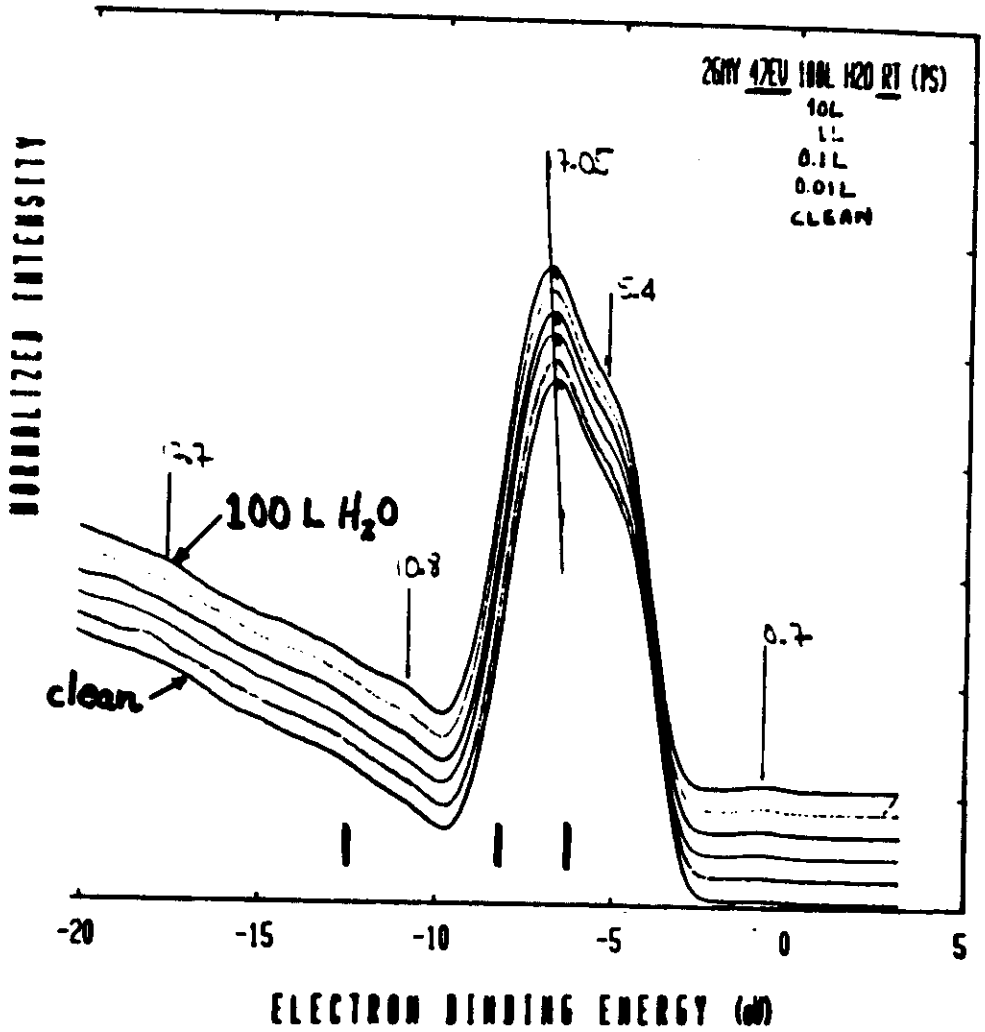

Interaction of H_2O with $La_{1.8}Sr_{0.2}CuO_4$ ($T_c \sim 40K$)

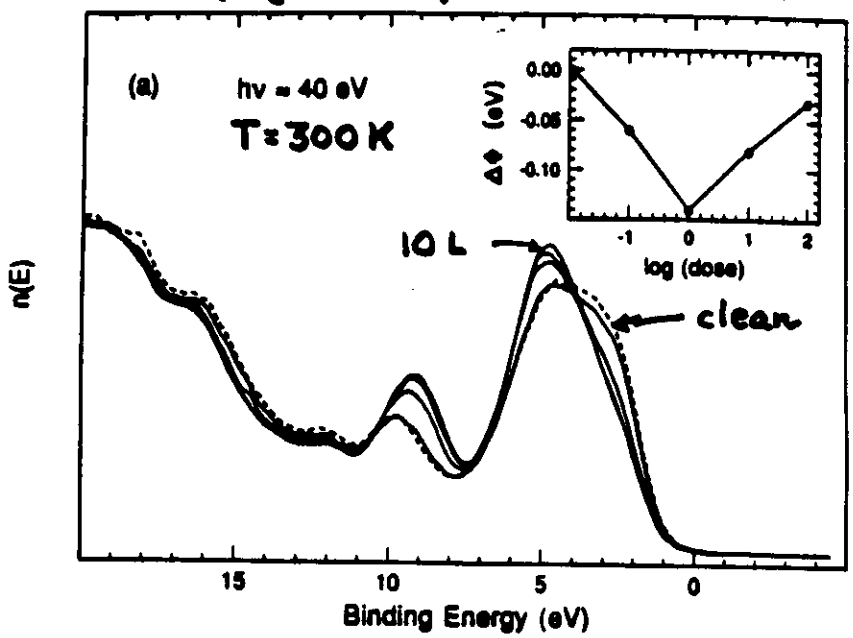

Difference Spectra

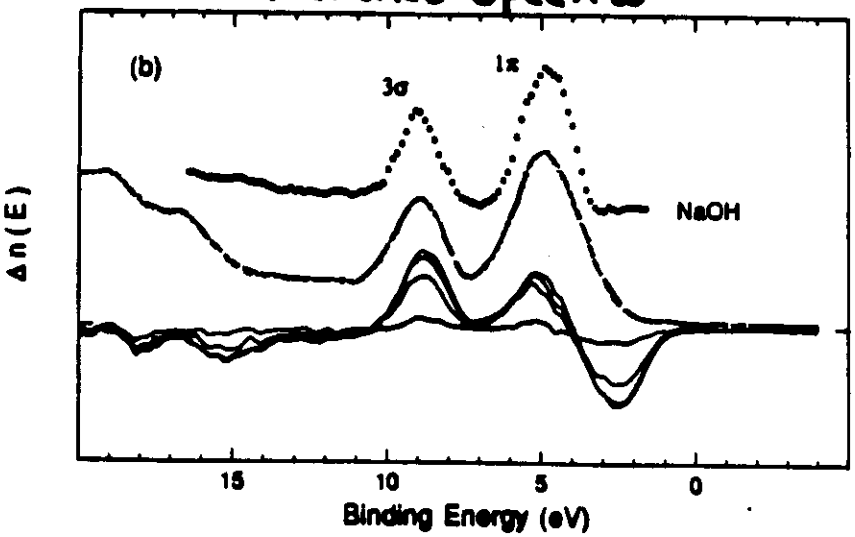

Summary

Strength of Adsorption Bond

- 50-80 kJ/mole
- Bonding via O Lone-Pairs
- No Adsorption in Vacuum, T≤300K

Structure of H_2O

- Long-Range and Azimuthal Order Greater for Strongly Bound H_2O

Influence of Additives

- Molecular Reorientations
- Long-Range Order
- Change Surface Chemistry

Oxides

- Material-Dependent Chemistry

IV. Specific Examples, continued.

The remainder of the lectures in this series will be concerned with additional examples of the structure of small molecules on metals and semiconductors, the structure of oxide surfaces, negative ion ESDIAD, and beam damage in surface analysis:

B. CO on Metals.

a. "Standing up" CO

- terminally bonded CO/Ru(001)
- terminally, bridge-bonded CO/Ni(111)
- virgin CO/W(110)
- dynamical effects in ESD ion yields: resonant charge exchange

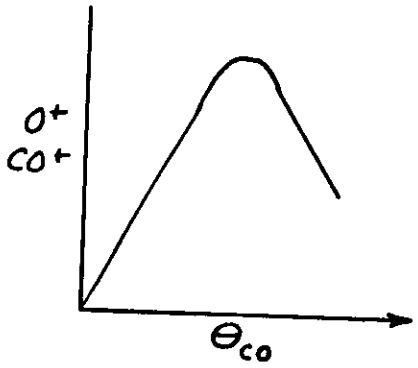

ESD of CO on
Ni(111)
Ru(0001)
W(110)
Pd(210)
and CO*/Ni(110)

At low θ_{CO}, adsorbate-substrate interaction dominates neutralization.

At high θ_{CO}, resonant charge exchange and band structure effects dominate.

b. "Inclined" CO

- CO/Pd(210): inclined, bridge-bonded CO

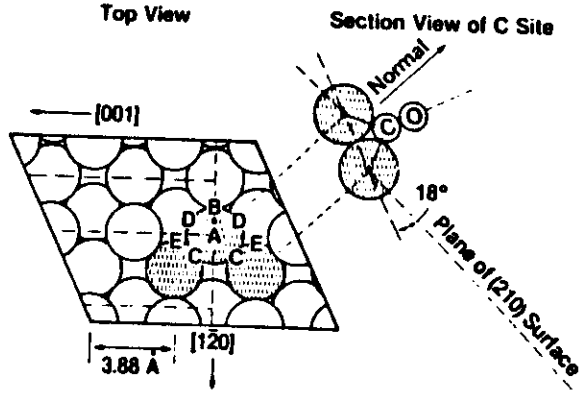

- CO/W(110) steps
- CO/Ni(110)
- CO/Cr(110) : EELS, UPS evidence
- CO + Na/Ru(001)

Key references to CO:

CO/Ni(111): F.P. Netzer, T.E. Madey, J. Chem. Phys. 76 710 (1982).

CO/Pd(210): T.E. Madey, J.T. Yates, Jr., A.M. Bradshaw and F.M. Hoffmann, Surface Sci. 89, 370 (1979).

CO/Ni(110): W. Riedl and D. Menzel, Surface Sci. 163, (1985); M.D. Alvey et al., ibid., 165, 447 (1986).

CO/Cr(110): N.D. Shinn and T.E. Madey, J. Chem. Phys 83, 5928 (1985).

C. NH_3 on Metals: role of impurities

a. Adsorption on clean surfaces

- NH_3 on Ru(0001), Ni(111), Ni(110), Ag(110)

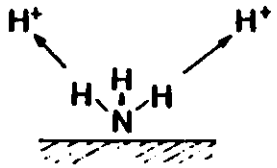

- NH_3 on stepped Fe(100): "inclined" molecules

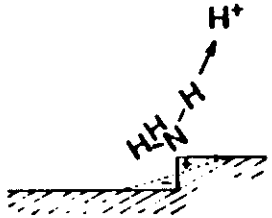

b. Influence of impurities on bonding of NH_3

- NH_3 + O on Ni(111), Ru(0001)

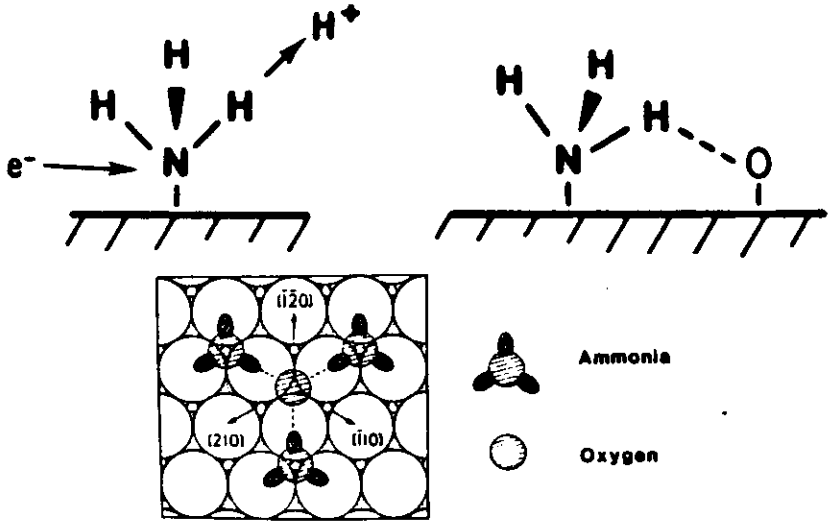

Model for the oxygen-induced azimuthal orientation of NH_3 on O/Ru(001).

- NH_3 + Na on Ru (0001), Ni(110).

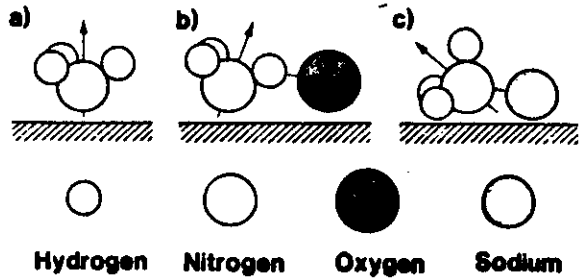

Key references to NH_3 on metals:

NH_3 Ni(110): F.P. Netzer & T.E. Madey, Surface Sci. 119, 422 (1982).

NH_3/Ru(001): C. Benndorf & T.E. Madey, Surface Sci. 155, 164 (1983); Chem. Phys. Lett. 101, 59 (1983).

NH_3/Fe(100): C. Benndorf, T.E. Madey, and A.L. Johnson, Surface Sci. 187, 434 (1987).

D. Adsorption on Silicon: H_2O and HF.

- Adsorption on Si(100): dissociation of H_2O, HF, NH_3 across the dimers.

Langmuir, Vol. 4, No. 2, 1988

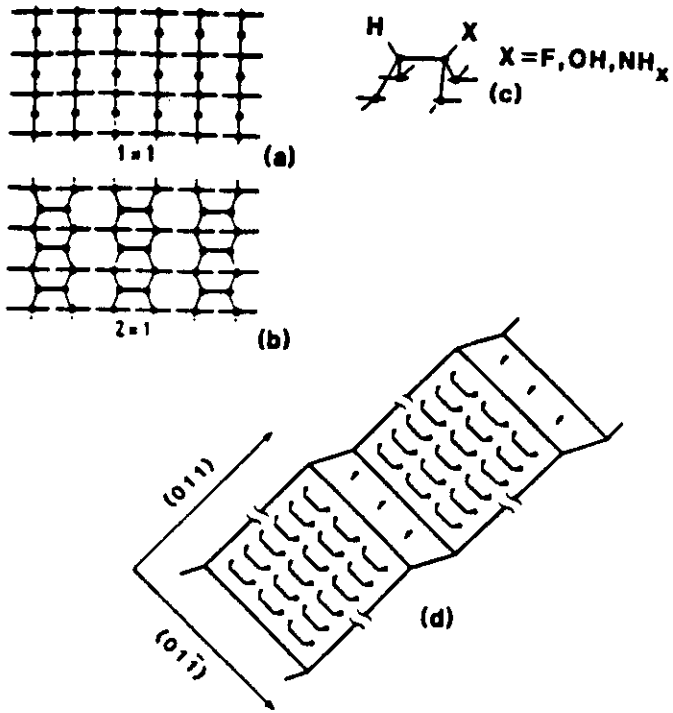

Figure 1. (a) Model of the unreconstructed Si(100) surface. (b) Model showing the formation of the rows of silicon dimers. (c) Model of the silicon dimer, showing dangling bonds and a model of the dissociative chemisorption of HF, H_2O, and NH_3. (d) Model of the stepped surface. Note the terraces of dimer rows, 22 in our case, with the dimers terminated by dangling bonds.

- Model for HF.

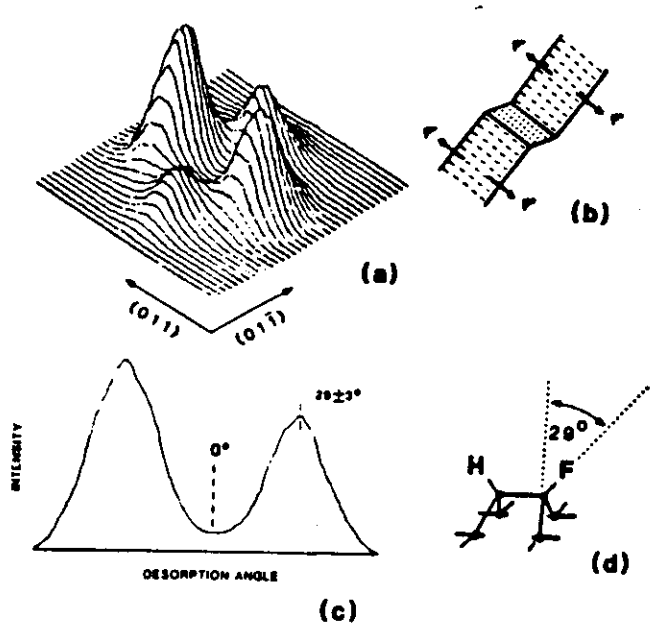

Figure 6. (a) ESDIAD of a saturation doses of HF on stepped Si(100) at 230 K. (b) Model showing that the F^+ emission is *parallel* to the surface dimers, i.e., along the azimuth of the Si–Si dimer bond. (c, d) The polar angle of the ion emission at 130 K (and thus the Si–F bond) is 29 ± 3° and the fwhm is 19°. Note that the ion emission peaks are sharp, indicating the silicon dimer is not in two different asymmetric forms. The intensity versus desorption angle plot, c, was taken with a compression field (due to a 80-V bias applied to the sample) and is a "slice" through the perspective plot a. The polar angle was determined in other experiments where there was no compression field.

Key reference:

A.L. Johnson, M.M. Walczak, T.E. Madey, Langmuir 4, 277 (1988).

E. PF_3 on Metals: Dynamical Effects

- PF_3 on Ni(111) and Ru(0001): hindered rotor

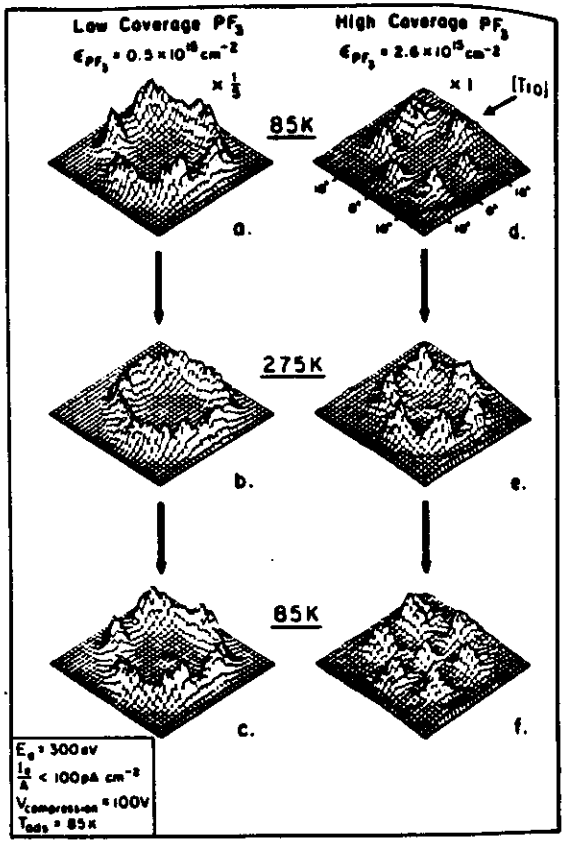

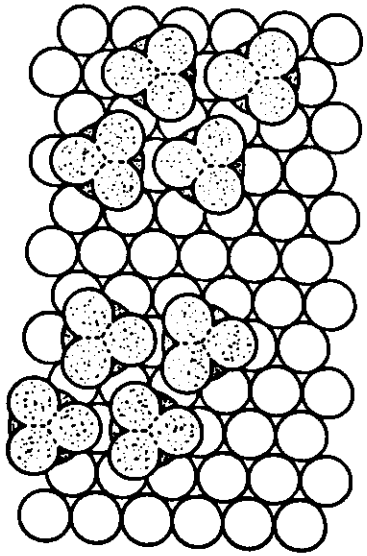

Key reference:

M.D. Alvey, J.T. Yates, Jr. and K.J. Uram, J. Chem Phys. 87, 7221 (1987).

F. Negative Ion (ESDIAD)

a. Test molecules: PF_3, $(CF_3)_2CO$, NF_3 on Ru(000

b. Method: time-of-flight

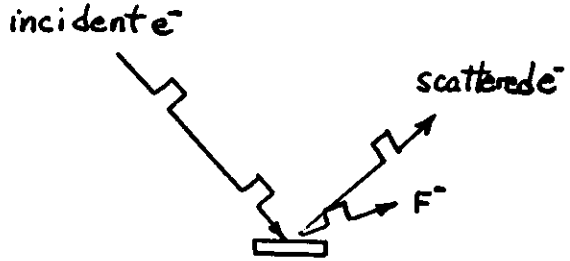

c. Results

- negative ions detected; yields comparable to positive ions

Ion Yields
(ions/electron)

	F^+ Yields	F^- Yields
PF_3/Ru(001)	1.4×10^{-4}	1.2×10^{-5}
NF_3/Ru(001)	2×10^{-5}	6×10^{-7}
HFA/Ru(001) (multilayer)	6×10^{-5}	3×10^{-4}
HFA/Ru(001) (monolayer)	4×10^{-5}	3×10^{-5}

- F^- ESDIAD gives highly structured patterns related to surface bonding geometry

F^- ESDIAD from PF_3/Ru(0001)

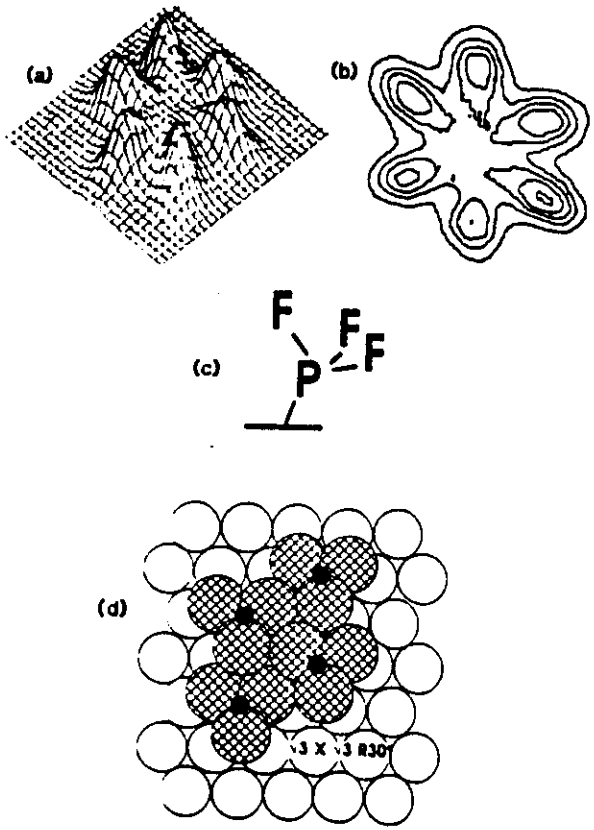

- Positive and negative ions give complementary information. Negative ions come mainly from undissociated molecules, positive ion yields are higher for dissociation fragments than for molecule.

PF_3 Temperature Dependence

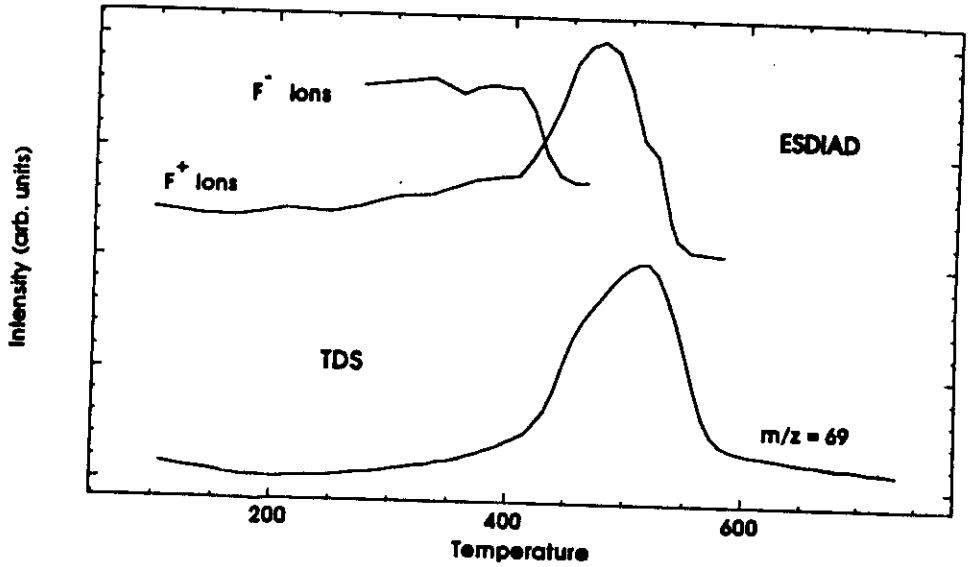

Negative Ion Formation Mechanisms

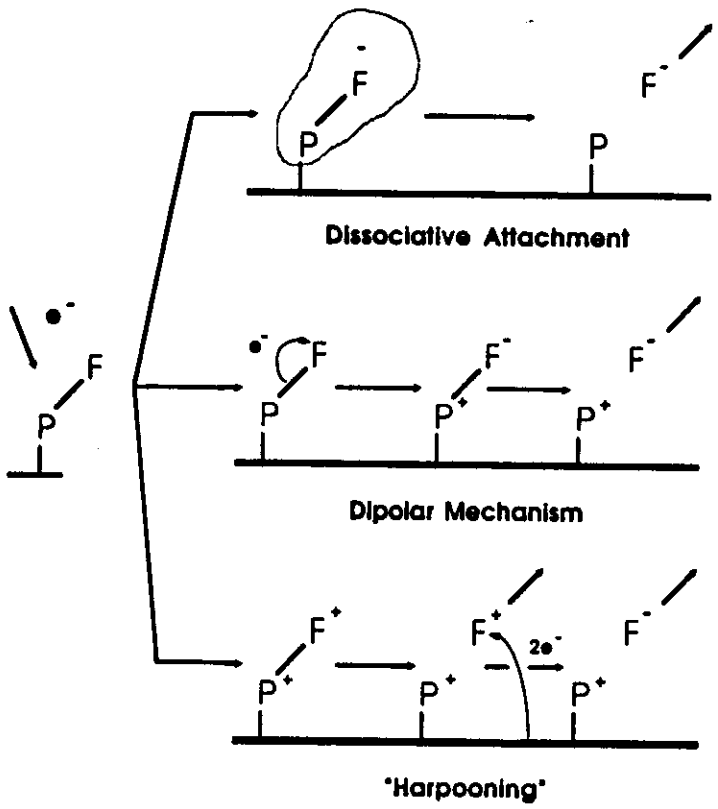

Key reference:

A.L. Johnson, S.A. Joyce, and T.E. Madey, Phys. Rev. Letter, in press.

G. Beam Damage in Surface Analysis.

Surface analysis techniques such as electron-excited Auger electron spectroscopy (AES) and x-ray photoelectron spectroscopy (XPS) are often plagued by radiation damage effects that change the surface structure and/or chemical composition. Damage-producing excitations compete with information-producing excitations in the surface layer during measurements, and the resultant beam damage can be a serious perturbation in quantitative surface analysis. The following aspects of radiation damage are discussed: (1) the role of valence- and core-electron excitations in bond-breaking and desorption, (2) cross sections for damage and the critical radiation dose for damage, (3) relative damage rates in AES and XPS, (4) examples of beam damage in surface analysis, and (5) remedies for minimizing beam damage.

References:

T. E. Madey, in D.C. Joy, editor, Analytical Electron Microscopy-1987 (San Francisco Press, 1987) p. 345

C. G. Pantano and T. E. Madey, Appl. Surface Sci. 7, 115 (1981).

Beam Damage in AES

Material	D_c(C/cm^2) $j_e \cdot t$	T(time)
Al_2O_3	10	3 h
Cu,Fe pthalocyanines	>1	>15 min
SiO_2	0.06	10 min
NaF, LiF	0.006	60 s
$LiNO_3$, $LiSO_4$	0.05	50 s
H_2O(F)	0.01	10 s
Native oxides	2×10^{-3}	2 s
C_6H_{12}(F)	3×10^{-4}	0.3 s
Na_3AlF_6	10^{-4}-10^{-3}	0.1 s
CH_3OH(F)	2.5×10^{-4}	0.3 s

(F): condensed film
D_c: the dose (C/cm^2) reported for beam-damage
T: the time in which damage will be detected under electron irradiation by 1mA/cm^2

What else is exciting about ESD/PSD?

1. Instrumentation

   -digital display (Sandia, Pitt, NBS)
   -ellipsoidal analyzer

2. New applications

   -substrate structure (oxides)
   -adsorption on oxides, semiconductors

3. Mechanistic studies

   -PSD : synchrotron radiation
     broad energy range, polarization
   -materials degradation
   -Dynamics:
     Desorption of negative ions, neutrals
     (including metastables)

4. Theory
   -classical and semiclassical
   -first principles calculations

Reprint Series
17 October 1986, Volume 234, pp. 316–322

SCIENCE

Electron- and Photon-Stimulated Desorption: Probes of Structure and Bonding at Surfaces

THEODORE E. MADEY

Electron- and Photon-Stimulated Desorption: Probes of Structure and Bonding at Surfaces

THEODORE E. MADEY

Techniques for analyzing the structure and composition of solid surfaces with electron and photon beams often cause radiation damage in samples. Damage-producing processes compete with information-producing events during measurements, and beam damage can be a serious perturbation in quantitative surface analysis. There are, however, substantial benefits of electron- and photon-stimulated damage processes for studying molecules adsorbed on surfaces. Direct information about the geometric structure of surface molecules can be obtained from measurements of the angular distributions of ions released by electron- or photon-stimulated desorption. The directions of ion emission are determined by the orientation of the surface bonds that are ruptured by beam irradiation. Moreover, photon-stimulated desorption studies that make use of synchrotron radiation reveal the fundamental electronic excitations that lead to bond-breaking processes at surfaces. These measurements provide new insights into radiation-damage processes in areas as diverse as x-ray optics and semiconductor electronics.

ELECTRONS AND PHOTONS ARE WIDELY USED AS PROBES for surface chemical and structural analysis in a number of surface measurements, including Auger electron spectroscopy, x-ray photoelectron spectroscopy, and scanning electron microscopy. The assumption in most of these studies is that the bombarding electrons and photons are relatively unperturbing probes that do little damage to the structure or composition of the surface being characterized. In fact, electron and photon bombardment can induce various bond-breaking processes at surfaces that are analogous to gas-phase electron- and photon-induced dissociation. In most surface analyses, this radiation-induced rupture of surface bonds is a nuisance to be avoided or minimized; in the cases described here, analysis of the surface dissociation (desorption) products can be beneficial by providing insights into the structure and bonding of surface species. This information comes from electron-stimulated desorption (ESD) and photon-stimulated desorption (PSD) studies of surfaces, which are the subject of much experimental and theoretical interest (*1–5*).

In ESD and PSD, beams of energetic electrons or photons (typically about 10 to more than 1000 eV) incident on surfaces

The author is an NBS fellow in the Surface Science Division at the National Bureau of Standards, Gaithersburg, MD 20899.

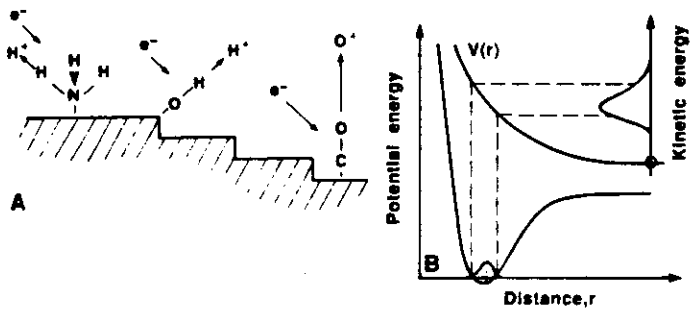

Fig. 1. (A) Schematic bonding configurations for adsorbed molecules on a stepped surface, showing the relation between surface bond angle and ion desorption angle in ESDIAD. The step heights have atomic dimensions. (B) Schematic potential energy diagram illustrating stimulated desorption of surface species. Electronic excitation from the attractive ground-state potential curve to the repulsive excited-state potential curve can lead to desorption of energetic species. $V(r)$ is the potential energy as a function of the atom-surface separation r.

containing terminal bulk atoms, or adsorbed monolayers of atoms or molecules, cause electronic excitations in the surface species. These excitations can result in desorption of ions, ground-state neutrals, or metastable species from the surface. Similarly, electronic excitation of bulk atoms can cause atom displacements, leading to radiation damage (such is the case in electron microscopy). A major difference that distinguishes ESD and PSD processes at surfaces and bulk radiation-damage events from gas-phase dissociative ionization processes is that the surface and bulk provide pathways for electronic deexcitation that are not available in the gas phase.

During the last few years, there have been substantial advances in understanding the mechanisms and extending the applications of ESD and PSD (*1–5*). Extensive theoretical work has provided new insights into the nature of the electronic excitations and the energy-localization processes that cause bond breaking and desorption (*6*). Angle-resolved ESD and PSD measurements are well-established tools for characterizing the geometry of surface molecules: ion desorption directions are related directly to the orientations of the ruptured bonds (*7, 8*). The use of synchrotron radiation to probe the thresholds and energy dependence of desorption has, in many cases, provided a detailed understanding of the multiple-electron excitations that induce desorption. Criteria have been recognized that govern the stability of surfaces to ionizing radiation (that is, radiation damage); this is a key issue in surface analysis (*9*).

This article examines the following aspects of the electron-surface and photon-surface interactions: (i) the basic physics of electron and photon bond-breaking interactions with surfaces, and how desorption is initiated; (ii) applications of ESD and PSD to surface science, with emphasis on the determination of molecular structure at surfaces by means of ESD ion angular distributions (ESDIAD); and (iii) the perturbing effects of electron and photon beams in surface analysis (*10*).

Basic Physics: Experimental Considerations

As a background for discussing the mechanisms of ESD and PSD, it is useful to summarize the basic experimental observations that characterize ESD and PSD measurements in the electron and photon energy range 10 to 1000 eV (*1–5*).

Desorption products. The observed ESD and PSD desorption products include positive and negative ions as well as ground-state neutrals and vibrationally and electronically excited neutrals (metastables). Because of their relative ease of detection, positive ions have been the focus of most ESD and PSD studies. For adsorbed monolayers of small molecules on surfaces, the most common ions observed are atomic (for example, H^-, O^-, F^+, Cl^+), but substantial quantities of molecular ions (OH^- and CO^+) are also seen. Generally, yields of positive ions are 10 to 100 times greater than yields of negative ions. For condensed multilayers, the dominant ions are generally atomic (for example, H^+ from condensed H_2O or CH_3OH), but complex polyatomic ions are also observed (with lower probability). Neutral desorption products include both atomic and molecular species; metastable atoms (Na* and Li*) and molecules (CO* and NO*) have been observed and characterized (*11–13*). The desorbing molecules are often vibrationally hot. Desorbing ions originate in the top one to two atomic layers of the solid surface.

Cross sections. The maximum cross sections for desorption of ions from surfaces ($\sim 10^{-20}$ to 10^{-23} cm^2) are generally smaller than those for the desorption of neutral species ($\sim 10^{-18}$ to 10^{-20} cm^2); both are smaller than typical cross sections for gas-phase dissociative ionization ($\sim 10^{-16}$ cm^2 for 100-eV electrons). For ESD, maximum ion yields are approximately 10^{-6} ions per incident electron; PSD ion yields are usually smaller, although a high PSD neutral yield of 10^{-2} atoms per photon has been reported for Li* from LiF (*11*). The cross sections for desorption of substrate ions are vanishingly small for metal surfaces but can be large for certain maximal valence oxides (such as TiO_2 and WO_3) (*4, 9*).

Threshold energies for desorption. The threshold energy for desorption of neutral molecules (*14*) can be as low as 5 eV; this correlates with a one-electron valence excitation of the adsorbate. Valence and shallow-core excitations (*15*), which lead to ion desorption, have thresholds of 15 eV or greater. Deep-core excitations [for example, C(1*s*) at 280 eV and O(1*s*) at 530 eV] also correlate with ion desorption thresholds because new desorption channels are opened (*16*). Multiply charged ions are also seen at energies above deep-core hole ionization energies.

Energies of desorption products. The most probable range of kinetic energies for ESD and PSD ions is 1 to 10 eV; energies as high as 15 eV have been reported. There are far fewer measurements of neutral products (*14*); their most probable energies are significantly lower ($\leq$1 eV). As indicated above, both vibrationally and electronically excited (metastable) species have been observed and characterized.

Sensitivity to bonding mode. ESD and PSD cross sections are sensitive to the mode of bonding of an atom or molecule to a surface. In general, the cross section for breaking an internal molecular bond in an adsorbed molecule is higher than that for breaking the bond to the substrate (for example, ESD of H^+ from OH bound through the oxygen atom has a much higher cross section than ESD of H^+ from adsorbed atomic hydrogen).

Ion angular distributions: relation to structure. The utility of ESD and PSD for determining the structure of surface species derives from the fact that ESD and PSD ions do not generally exhibit isotropic distributions. Instead, they desorb in discrete cones of emission in directions determined by the orientation of the surface molecular bonds that are ruptured by electronic excitations. For example, as indicated schematically in Fig. 1A, ESD of CO bound in a "standing up" configuration on a metal surface will result in desorption of O^+ in the direction of the surface normal; ESD from "inclined" OH, or of H^+ from NH_3 adsorbed through the nitrogen atom, will occur in off-normal directions. Thus, measurements of the ESDIAD patterns yield direct information about the geometric structure of molecules in surface layers (*3, 7, 8*). Angle-resolved PSD contains similar information, but because of experimental difficulties it is less widely used. Angle-resolved desorption of neutrals and metastables has also been reported (*12*).

ESD and PSD similarities and differences. ESD and PSD are thought to be initiated by essentially the same elementary electronic

excitation of the surface (*4*). The equivalence of ESD and PSD excitations has been demonstrated through similarities in desorption threshold energies, in ion energy distributions, in ion angular distributions, and in the nature of the surface species from which desorption occurs. There are differences, however, in the shapes of the ESD and PSD spectral yield curves (ion yield compared to excitation energy) and in the magnitudes of the excitation cross sections for electron and photon excitation. A PSD ion yield curve generally has a sharp threshold that is followed by a maximum and a relatively abrupt decay of the signal. In contrast, ESD spectra have weak thresholds and rise smoothly above threshold. The origin of these spectral shapes and the relevant excitation physics have been discussed (*4*).

Mechanisms of ESD and PSD

It is clear from the data described above that stimulated desorption is initiated by an electronic excitation of a surface molecular bond: neither thermal effects nor direct momentum transfer (such as that between a bombarding electron and a surface atom) can account for the low threshold energies and the observation of massive ions with high kinetic energies.

Stimulated desorption is usually described in terms of specific models, such as the Menzel-Gomer-Redhead model of desorption from covalent adsorbates (*17*) or the Knotek-Feibelman model of desorption from ionic substrates (*9*). In the former model, the primary process is a Franck-Condon excitation or ionization to a repulsive neutral or ionic state, from which desorption can occur. The latter model is particularly applicable to highly ionic systems and is based on the ionization of a core level as the primary process. The interatomic Auger decay of the core hole creates a positive ion at an initially negative ion site, and the expulsion of the positive ion results from the reversal of the Madelung potential. A more generalized Auger-stimulated desorption model has been described (*18*) that extends the Knotek-Feibelman model to less ionic and covalent systems.

Although these models differ in detail, they have much in common. The essential features of the stimulated desorption excitation process, as embodied in all the models, can be described approximately (*3, 6*) as a sequence of three processes (Fig. 1B), as follows: (i) a fast initial electronic excitation ($\sim 10^{-16}$ second) (typically this is a valence or core excitation); (ii) a fast electronic rearrangement ($\sim 10^{-15}$ second) to a repulsive electronic state having a lifetime of about 10^{-14} second (repulsive electronic energy is converted to nuclear motion); and (iii) a modification of the desorbing species (its energy, charge state, or trajectory) as it leaves the surface.

As illustrated in Fig. 1B, the surface bond is excited by electron or photon excitation through a valence or core hole ionization process (on a time scale of about 10^{-16} second). For valence excitations involving one-electron processes, excitation can be direct to a long-lived (10^{-15} to 10^{-14} second) antibonding repulsive state, from which desorption can occur. This can be a major route to desorption of ground-state and excited neutral species. It is widely believed (*3–6*) that ESD and PSD of ions from both covalently bonded and ionically bonded surface species proceed through multielectron excitations that produce two-hole (2h) or two-hole, one-electron (2h1e) excited states. These excited states can be highly repulsive, with hole localization lifetimes on the order of 10^{-14} second, so that the repulsive electronic energy can be converted to nuclear motion. For example, an 8-eV O^+ ion will travel about 1 Å in 10^{-14} second, so that the surface bond is effectively broken. This process is an important route to ionic ESD and PSD products.

The repulsive interaction in the excited electronic state (Fig. 1B) can be described as coulombic in origin and is directed primarily along the direction of the bond that is ruptured by the excitation. Hence, the initial ion desorption angle in ESDIAD is determined by the ground-state surface bond angle. There are, however, final-state effects [process (iii) above] that can influence ion desorption trajectories and yields; these include the surface image force and reneutralization effects (*19*). The image force invariably causes an increase in the polar desorption angle of an ion leaving a planar surface (that is, the trajectory is bent toward the surface). Reneutralization effects (electron hopping to the desorbing species by resonant tunneling or Auger neutralization) also influence the measured ion angular distributions and yields. Recent calculations indicate that, in addition, dynamical distortions of the substrate lattice after the initial excitation can influence the desorption processes (*20*).

Instrumentation

The ideal apparatus for stimulated desorption measurements is complex, having capabilities for independent control of a wide range of parameters in an ultrahigh vacuum (UHV) environment. Such an ideal apparatus (Fig. 2a) would permit measurement of the mass, desorption angle, kinetic energy, and internal energy (electronic, vibrational, and rotational) of ions and neutral species (*4*). All these properties would be studied as a function of the energy, angle of incidence, and polarization of the incident electron or photon beam, and the surface temperature would be controlled to influence surface chemistry; all this would take place at pressures of 10^{-10} torr or less. In addition, probes for characterizing the composition and structure of the surface, such as Auger electron spectroscopy and low-energy electron diffraction (LEED), would be available.

Figure 2b illustrates a UHV system constructed at the National Bureau of Standards for ESD of ions; this system permits mass and energy analysis of desorbing ions (by means of a mass spectrometer and retarding grids, respectively) as well as measurements of the ESDIAD patterns (*8*). A focused electron beam bombards a single crystal sample. The ESD ion beams pass through hemispherical grids and strike the front surface of a double microchannel plate assembly. The output signal from the assembly is accelerated to a fluorescent screen, where it is displayed visually (the ESDIAD pattern). By changing potentials, the elastic LEED pattern from the sample can be generated and observed. The ESDIAD and LEED patterns can be photographed (as has been done in most ESDIAD studies), or they can be recorded with a high-sensitivity video camera and a computer-controlled digital imaging processing system (*21*). The system at the National Bureau of Standards allows acquisition of real-time images or digitization of photographic negatives. Other features include creation of histograms and contour plots of ion intensity as a function of position on the detector and manipulation of the digital image (background subtraction, smoothing, and the like). Other digital imaging ESDIAD systems based on scanning collectors or resistive anode detectors are in use at Jülich (*22*), Sandia (Livermore) (*23*), and the University of Pittsburgh (*24*).

Applications of ESD/PSD to Surface Science

In surface science applications, ESD and PSD are among the few techniques that are sensitive to the presence of hydrogen at surfaces: the yields of H^+ from hydrogen-containing molecular fragments are generally high. Measurements of the energy thresholds for desorption provide bond-specific information; for example, one can distin-

guish among H^+ originating from adsorbed OH, CH, NH, or adsorbed hydrogen. PSD ion yields have been used as SEXAFS (surface extended x-ray absorption fine structure) probes in synchrotron radiation experiments (*25*) to determine surface structure (nearest-neighbor bond lengths).

Moreover, studies of radiation-induced bond-breaking processes at surfaces provide a detailed view of radiation damage mechanisms. Measurements of the yields and energy states of ions, ground-state neutrals, and metastable species that desorb from surfaces can give information about the initial excitations that can occur deep in bulk solids, although the bulk excitation may subsequently be quenched by efficient energy transfer processes. These studies provide a fundamental basis for understanding such phenomena as radiation damage in electron microscopy and the activation of photoresists or electron beam resists (*26*). Even ion bombardment of solids, in which the dominant damage mechanism is through momentum transfer, can cause damage by electronic excitations (*27*).

ESDIAD. By now, there is a wealth of experimental and theoretical evidence that the direction of ion emission is related directly to the orientation of the surface bond that is ruptured by the excitation.

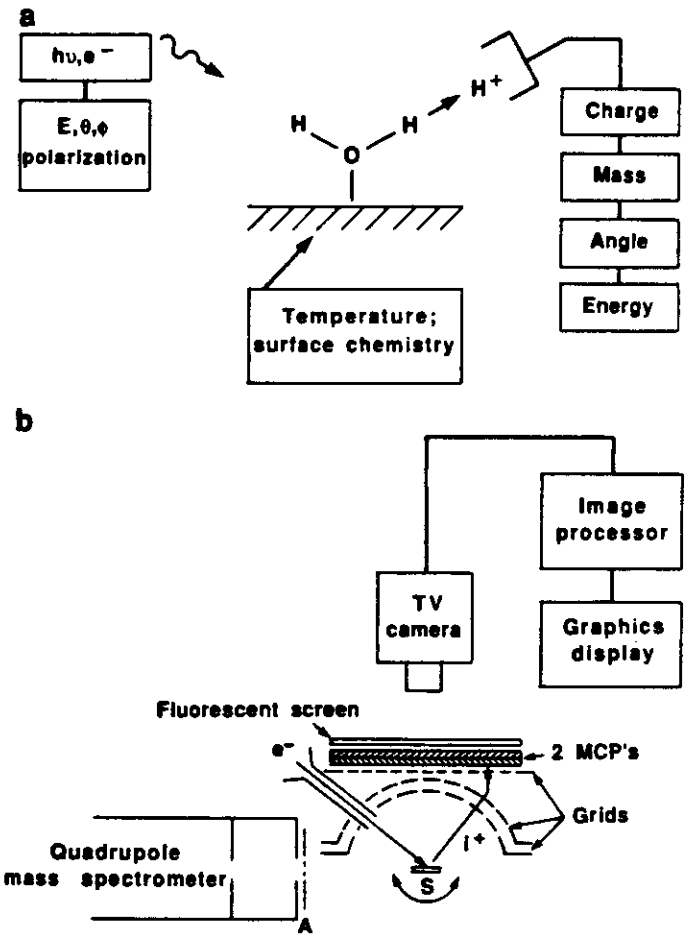

Fig. 2. (a) Ideal stimulated desorption apparatus, in which one has control over the energy (E), angle of incidence (θ, ϕ), and polarization of the incident radiation; the ability to measure the mass, angle, and kinetic and internal energy of the desorbed ions or neutrals; and the additional ability to characterize the surface and to control the surface chemistry. [From (*4*)] (b) An imaging ESDIAD apparatus for measuring ion angular distributions. The grids are used to accelerate ions. The ion signal is amplified with the microchannel plates (MCP), and the secondary electrons from the MCP's are accelerated to the fluorescent screen, where they produce light pulses. The resulting ESDIAD pattern can either be photographed or detected with a video camera. The images are digitized and processed by means of a computer graphics system (*8, 21, 33*). Abbreviations: S, source; A, aperture.

Although there are effects (image force and reneutralization) that can alter the desorbing ion trajectories (*19*), there is a great deal of qualitative and quantitative structural information (in particular, information about bond angles) available in ESDIAD measurements. The structures of atoms and molecules adsorbed on metals (*8*) and of clean oxide substrates have been reported (*15*).

There are many ESDIAD results (*8*) that confirm molecular structural assignments (for example, for CO, NO, NH_3, H_2O, and C_6H_{12} adsorbed on metal surfaces) made by means of other surface-sensitive techniques. The observations that molecular CO "stands up" on Ni(111) and Ru(001) surfaces (bound through the carbon atom with the molecular axis perpendicular to the surface plane), that it "lies down" on Cr(110) (with the molecular axis parallel to the surface), and that it is "inclined" on surfaces such as Pd(210) illustrate the complexities of bonding for one molecule in different environments. In a recent example (*28*), CO on Ni(110) was found to bond in a "standing up" configuration for CO coverages below about 0.75 monolayer. At higher coverages, up to one monolayer, lateral repulsive interactions between neighboring molecules force the CO into "tilted" configurations, with the molecular axes inclined 19° from the surface normal. Polar molecules such as NH_3 and H_2O are found to bond to many surfaces through the lone pair orbitals on the nitrogen or oxygen atoms, with the hydrogen atoms pointing away from the surface: the binding structures have been determined directly in many ESDIAD experiments (*8*).

Azimuthal ordering in adsorbed overlayers. There is one area in which ESDIAD has provided a detailed new view of structure and bonding on surfaces: the interaction of small molecules (NH_3, H_2O, CO) with adsorbed impurity atoms (O, Br, Na, K) on metal surfaces (*8, 29*). As a result of interaction with the adsorbed additive atom, the surface molecule is often reoriented into a bonding structure different from its local structure in the absence of the additive. For example, a fractional monolayer of preadsorbed oxygen on a Ni(111) surface can induce a high degree of local azimuthal ordering in adsorbed NH_3 and H_2O, even though these molecules have random azimuthal orientations on the clean nickel surface (*29*). In most cases, it appears that the molecule-additive interaction is a short-range, local interaction occurring at nearest-neighbor distances; hydrogen bonding and other electrostatic effects have been postulated.

An example of the influence of electronegative surface additives (Br, O) on the structure and chemistry of H_2O adsorbed on Ag(110) is illustrated in Fig. 3. The objective of the work from which this example derives was to provide a synthetic version of the electrochemical "double layer" that exists at the interface between electrode and electrolyte in an electrochemical cell. The interface simulation was accomplished by adsorbing, in UHV, controlled amounts of bromine and oxygen atoms as well as solvent H_2O molecules onto an initially clean Ag(110) surface (*30*).

Figure 3A shows perspective and contour plots of the H^+ ESDIAD pattern for fractional monolayers of H_2O adsorbed on Ag(110) at 80 K. For adsorbed H_2O, the dominant ESD ion is H^+ from rupture of OH bonds. The random emission centered about the surface normal (center of the pattern) indicates that the adsorbed H_2O is disordered locally; there is no long-range order at any coverage, as determined by LEED. These and other measurements indicate that H_2O is adsorbed in poorly ordered hydrogen-bonded clusters on Ag(110) at 90 K.

In contrast to this situation, the interaction of H_2O with a preadsorbed fractional monolayer of bromine or oxygen atoms on Ag(110) causes the clusters to break up: new surface structures are formed. On bromine-dosed Ag(110), a surface hydration shell containing two H_2O molecules is believed to form around each adsorbed bromine atom. Evidence for a pronounced orientational

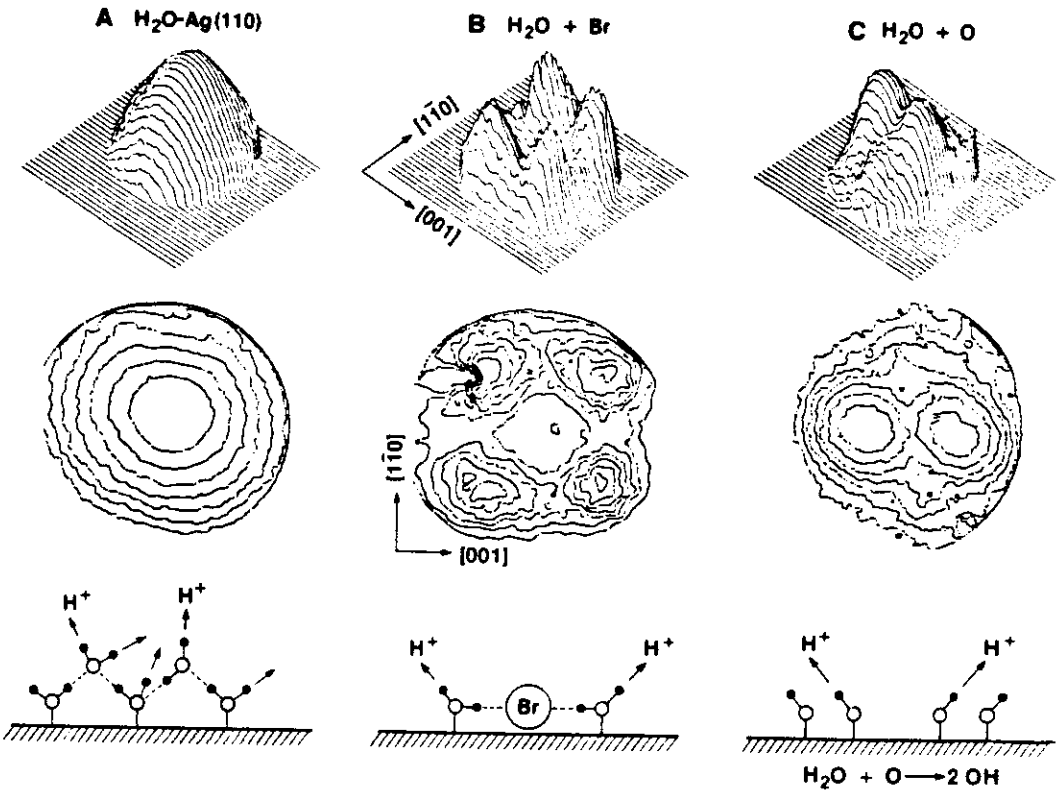

Fig. 3. H^+ ESDIAD patterns and schematic models illustrating the influence of bromine and oxygen on the local structure of H_2O on the Ag(110) surface (*30, 31*). The top row contains perspective plots of the ion intensity displayed on the fluorescent screen of Fig. 2b. The second row contains contour plots of ion intensity for the same measurements as the top row. The third row contains schematic molecular models. (A) H^+ ESDIAD and models for H_2O on clean Ag(110). (B) H^+ ESDIAD and models for H_2O + Br on Ag(110). (C) H^+ ESDIAD and models characteristic of H_2O + O on Ag(110).

ordering of the H_2O molecules adjacent to the bromine is seen in Fig. 3B, where a distinct four-beam H^+ ESDIAD pattern is displayed. A model in which the adsorbed H_2O is stabilized by a hydrogen-bonding interaction with adsorbed bromine has been proposed (*30*); a simplified schematic picture is given at the bottom of Fig. 3.

As shown in Fig. 3C, a very different orientational ordering is found for H_2O adsorbed on oxygen-dosed Ag(110). In this case, the dominant H^+ beams are oriented along [001] azimuths, with weaker beams along [1$\bar{1}$0] azimuths (*31*). H_2O is known to dissociate on oxygen-dosed Ag(110) to form adsorbed OH species [H_2O + O (adsorbed) → 2 OH (adsorbed)], even at cryogenic temperatures. As shown in the lower part of Fig. 3C, the OH species are tilted along [001] azimuths, giving rise to the intense ESDIAD beams in the top part. The weaker beams along [1$\bar{1}$0] azimuths are due to OH-stabilized H_2O.

The dramatic influence of both bromine and oxygen on the structure and chemistry of H_2O on Ag(110) is not an isolated case. There are many examples in which additive atoms exhibit strong effects on adsorbed molecular structures (*8, 29*). This phenomenon—additive-induced changes in bonding geometry—may be related to the mechanisms by which catalyst promoters and poisons influence catalytic reaction pathways.

ESDIAD of H_2O on Si(100): influence of surface vibrational dynamics. Although extensive ESDIAD measurements have been made for adsorbates on metal surfaces, there have been few ESDIAD data reported to date for adsorbates on semiconductors (*15*). One important problem addressed at the National Bureau of Standards concerns the interaction of H_2O with silicon surfaces; the technological importance of this interaction with respect to the wet oxidation process is motivation for understanding the details of the H_2O-Si surface chemistry (*32*).

Although there has been some controversy concerning the state of adsorbed H_2O on silicon at 300 K (is it molecular, or does it dissociate into H + OH?), the strongest evidence is in favor of dissociative adsorption (*32*). The Si(100) surface is believed to undergo a reconstruction involving the formation of surface dimers, and it has been proposed that H_2O dissociates to OH and H bonded to opposite ends of the surface dimer (Fig. 4).

Figure 4 illustrates ESDIAD perspective and contour plots for H_2O adsorbed on a planar Si(100) surface at 300 and 140 K (*33*). It was found in separate experiments that the only ionic desorption product was H^+ and that the H^+ yield from adsorbed OH was substantially higher than that from adsorbed hydrogen. Several facts are evident from Fig. 4. First, there is an emission minimum in the center of the pattern in the direction of the surface normal, so that the OH are tilted with respect to the normal. Second, the pattern at 140 K contains four clearly resolved maxima along [011] azimuths, whereas the pattern at 300 K is less well resolved and has a doughnutlike appearance. The four-lobed pattern arises from two domains of Si(100) dimers, rotated by 90° from one another. The temperature dependence is completely reversible as the sample is heated or cooled between 140 and 300 K.

The reversible temperature dependence of the ESDIAD patterns indicates that the inclined OH species are not rigidly fixed on Si(100) in a few distinct orientations but that they undergo considerable surface motion—in particular, large-amplitude, low-frequency hindered rotations and bending and wagging modes. The ESDIAD pattern represents a "snapshot," at a particular temperature, of the distribution of OH bond orientations measured with respect to the surface normal (*8, 34*). From the temperature dependence, the frequency of the bending and wagging modes is less than 100 cm^{-1}, which is comparable to measurements made on ligands in gaseous molecular complexes.

Summary of information from ESDIAD. Some of the uses of ESDIAD in surface science can be summarized as follows. (i) ESDIAD provides direct information regarding surface molecular structures: ion desorption angles are related to surface bond angles. ESDIAD is not a diffraction technique; real-space images of bond directions are observed. (ii) ESDIAD is sensitive to bond orientation, that is, to the local bonding geometry. Long-range order in the surface adlayer is not necessary to produce an ordered ESDIAD

pattern. (iii) ESDIAD is especially sensitive to the orientation of hydrogen atoms in surface molecular complexes. In contrast, LEED is relatively insensitive to the positions of hydrogen atoms in adsorbed molecules. (iv) Finally, ESDIAD is particularly helpful when used in conjunction with other surface-sensitive techniques. Whereas bond directions are determined with ESDIAD, quantitative measurement of the bond length requires a technique such as SEXAFS. Whereas ESDIAD is sensitive to the local order, LEED is sensitive to the long-range order in the surface layer. Vibrational spectroscopy, such as high-resolution electron energy loss spectroscopy, is extremely important for identifying the stoichiometry of surface molecular complexes whose structures are studied by ESDIAD.

ESD and PSD as Perturbations in Surface Analysis: Beam Damage

Care must be taken to minimize or control damage effects when characterizing surface composition, structure, or topography by techniques that involve electron beams (*10, 35, 36*). There are several causes of beam-induced damage in surface analysis (*10, 36*). The first and most important arises from the bond-breaking electronic excitations discussed earlier. Deep-core and valence electronic excitations induced by both the primary electron beam and the secondary electrons released from the sample can cause desorption of surface species, leading to rapid changes in chemical composition and even structure of the surface and near-surface regions. In general, an electron or photon beam incident on oxides and practical surfaces in UHV is a reducing agent. A related effect is electron-stimulated adsorption, in which gaseous molecules adsorbed on the surface are "cracked" by the electron beam, resulting in accumulation of a surface residue. A frequently observed example of this process is the carburization or carbon buildup that occurs on samples in electron microscopes operated in background pressures of 10^{-6} to 10^{-7} torr of hydrocarbon vapors (not UHV). If the background gas contains substantial quantities of H_2O, samples can also be oxidized during electron bombardment.

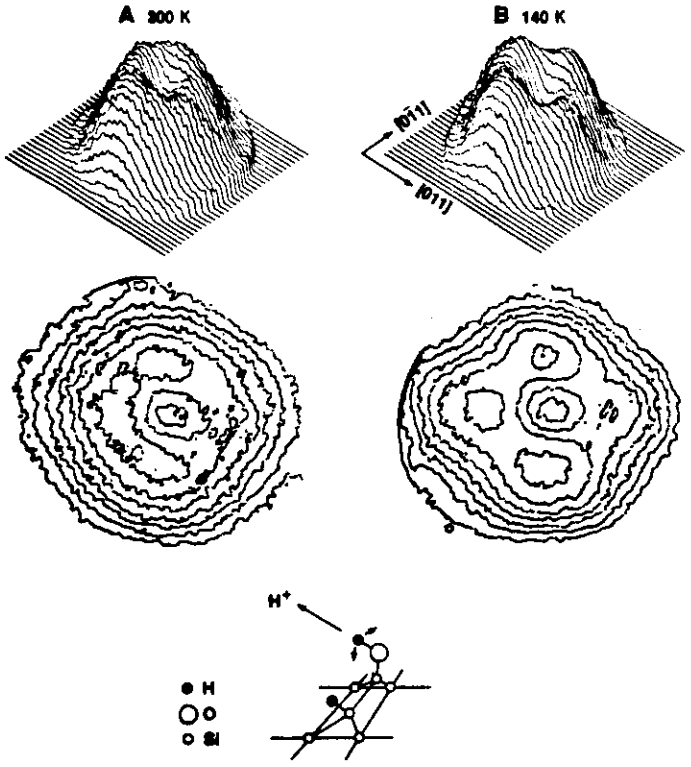

Fig. 4. H^+ ESDIAD and schematic models illustrating the bonding of OH to a Si(100) surface (*33*). (A) H^+ ESDIAD (perspective and contour plots) at 300 K; (B) H^+ ESDIAD at 140 K. A schematic bonding model in which H and OH are bound to both ends of a Si(100) dimer (*32*) is shown at the bottom. The four H^+ beams in (B) are due to ESD from degenerate dimer configurations. The decrease in resolution of ESDIAD at 300 K is due to increased vibrational motion of the OH species.

A second effect is the local heating that can be induced by the primary electron beam (typically 1 to 100 μA and 2 to 5 keV for Auger spectroscopy). The beam is usually highly focused, and the power density can be high (tens of watts per square centimeter for typical Auger spectroscopy). Beam heating is a particular problem when studying insulators, especially powders: it is common to see small particles glowing incandescent during Auger analysis. Undesirable surface chemical reactions, volatilization, surface diffusion, or segregation can be a consequence. In general, the heating becomes more severe as spatial resolution is increased (because of the more highly focused beam). Another beam-induced problem is the surface charging of insulating samples during beam irradiation. Depending on the value of the secondary electron yield, the resultant surface potential can be either positive or negative. In addition to perturbing the measured spectra, the surface charge can cause the electric field–induced diffusion of mobile ions in insulators (an example is electron beam–induced diffusion of Na^+ through soda-lime-silicate glass).

Beam damage effects are usually much worse when using electrons (Auger spectroscopy, LEED, and scanning electron microscopy) than when using photons (x-ray photoelectron spectroscopy). For useful signal-to-noise in all these measurements, the electron flux used in the electron spectroscopies is normally much higher than the photon flux used in the photoelectron spectroscopy. In addition, the damage probability per incident electron is greater than per incident photon.

Which materials are most susceptible to beam damage? Organic materials, biological samples, condensed molecular films, and adsorbed polyatomic molecules are most fragile under electron or photon irradiation. Saturated hydrocarbons are more fragile than molecules with unsaturated bonds. In many of these cases, the beam-induced dissociation probability is similar to that for the isolated gaseous molecule, and it is difficult or impossible to make a measurement without causing damage. There are, however, materials for which increasing the damage caused by electron and photon bombardment is desired: these are the electron- and photon-beam resists used in modern lithography in microelectronic device fabrication (*25*).

Inorganic materials such as oxides and alkali halides are also subject to damage. Knotek and Feibelman (*9*) provided criteria for the stability of ionically bonded solids bombarded by ionizing radiation. The materials most likely to decompose under electron bombardment are maximal valency compounds, in which the cation and anion have large Pauling electronegativity differences. Such materials include TiO_2, V_2O_5, WO_3, MoO_3, SiO_2, and Al_2O_3. The desorption mechanism is initiated by a core hole on the cation with a subsequent interatomic Auger process and the desorption of O^+. Loss of oxygen leads to a reduction of the surface oxide. Nonmaximal valency oxides (NiO, FeO) are much more stable (*19*). Alkali halides are strongly affected by electron bombardment: at ambient temperatures, loss of halogen is the dominant damage process.

Metallic samples are not, in general, subject to significant beam damage: electronic excitations of surface and substrate atoms are rapidly screened by conduction electrons. As mentioned above, however, clean metals can quickly become covered by impurities as a result of electron-stimulated adsorption.

There are several "tricks" that can minimize beam damage in surface analysis. By using a defocused beam or by rastering (scanning) the probed beam rapidly over a large area, the total beam dose can be reduced. In addition, a homogeneous sample can be moved during analysis to expose fresh regions to the beam. Thus important compromises must be made in practical surface analysis between the precision and sensitivity of the analysis and the spatial resolution. Other techniques for reducing damage during analysis have been described (*36*).

Surface analysis is not the only area of science and technology where radiation-induced surface processes are a problem. Photon-stimulated desorption of gases from vacuum walls is a limiting factor in attaining UHV in high-energy synchrotron radiation sources; both ESD and PSD can cause injection of impurities into the plasma discharge from the walls of fusion reactors; stimulated desorption processes have been identified as potential damage mechanisms in ultraviolet laser optical components (*37*); and the photon-induced damage of substrates and thin film coatings is a vexing problem.

Conclusion

This article has had a limited objective, namely, to introduce scientists to some of the benefits and liabilities of ESD and PSD. The emphasis has been on physical concepts and applications of these techniques rather than on a quantitative discussion of mechanisms.

There are many challenges and much excitement in ESD and PSD. The use of high-flux, polarized synchrotron radiation at high photon energies (≫500 eV) is stimulating studies of surfaces and adsorbates in the energy range of deep cores. Although most ESD and PSD studies have focused on ions, measurements of the internal energy and angular distributions of neutrals (and metastables) are appearing. The expanding interest in ESD and PSD mechanisms and fundamental excitations should have increasing impact on technology in areas as diverse as x-ray optics, electron beam lithography, and electron microscopy.

REFERENCES AND NOTES

1. N. H. Tolk, M. M. Traum, J. C. Tully, T. E. Madey, Eds., *Springer Ser. Chem. Phys.* **24**, 1 (1983).
2. W. Brenig and D. Menzel, Eds. *Springer Ser. Surf. Sci.* **4**, 1 (1985).
3. T. E. Madey, D. E. Ramaker, R. L. Stockbauer, *Annu. Rev. Phys. Chem.* **35**, 215 (1984).
4. M. L. Knotek, *Phys. Scr. T* **6**, 94 (1983); *Rep. Prog. Phys.* **47**, 1499 (1984); *Phys. Today* **37**, 24 (September 1984).
5. D. Menzel, *J. Vac. Sci. Technol.* **20**, 538 (1982); *Nucl. Instrum. Methods B* **13**, 507 (1986).
6. D. R. Jennison, *Springer Ser. Chem. Phys.* **24**, 26 (1983); J. C. Tully, *ibid.*, p. 31; R. Gomer, *ibid.*, p. 40; P. J. Feibelman, *ibid.*, p. 61; D. E. Ramaker, *ibid.*, p. 70; N. D. Lang, *Springer Ser. Surf. Sci.* **4**, 2 (1985); D. E. Ramaker, *ibid.*, p. 10; D. R. Jennison, *ibid.*, p. 24; E. B. Stechel, *ibid.*, p. 32; J. Rubio *et al.*, *ibid.*, p. 40.
7. J. J. Czyzewski, T. E. Madey, J. T. Yates, Jr., *Phys. Rev. Lett.* **32**, 777 (1974); T. E. Madey and J. T. Yates, Jr., *Surf. Sci.* **63**, 203 (1977).
8. T. E. Madey, *Springer Ser. Chem. Phys.* **17**, 80 (1981); T. E. Madey, F. P. Netzer, J. E. Houston, D. M. Hanson, R. Stockbauer, *ibid.* **24**, 120 (1983); T. E. Madey, C. Benndorf, N. Shinn, Z. Miskovic, J. Vukanic, *Springer Ser. Surf. Sci.* **4**, 104 (1985); T. E. Madey, *J. Vac. Sci. Technol. A* **4**, 257 (1986).
9. M. L. Knotek and P. J. Feibelman, *Phys. Rev. Lett.* **40**, 964 (1978); *Surf. Sci.* **90**, 78 (1979).
10. A. Van Oostrom, *Surf. Sci.* **89**, 615 (1979); C. G. Pantano and T. E. Madey, *Appl. Surf. Sci.* **7**, 115 (1981); R. G. Copperthwaite, *Surf. Interface Anal.* **2**, 17 (1980).
11. N. H. Tolk *et al.*, *Springer Ser. Chem. Phys.* **24**, 156 (1983).
12. M. D. Alvey, M. J. Dresser, J. T. Yates, Jr., *Phys. Rev. Lett.* **56**, 367 (1986).
13. A. R. Burns, *ibid.* **55**, 525 (1985).
14. P. Feulner, R. Treichler, D. Menzel, *Phys. Rev. B* **24**, 7427 (1981); P. Feulner, *Springer Ser. Surf. Sci.* **4**, 142 (1985).
15. R. L. Kurtz, R. Stockbauer, T. E. Madey, *Nucl. Instrum. Methods B* **13**, 518 (1986).
16. R. Jaeger, J. Stohr, R. Treichler, K. Baberschke, *Phys. Rev. Lett.* **47**, 1300 (1981).
17. D. Menzel and R. Gomer, *J. Chem. Phys.* **41**, 3311 (1964); P. A. Redhead, *Can. J. Phys.* **42**, 886 (1964).
18. D. E. Ramaker, *Springer Ser. Chem. Phys.* **24**, 70 (1983); *Springer Ser. Surf. Sci.* **4**, 10 (1985); *J. Vac. Sci. Technol. A* **1**, 1137 (1983).
19. Z. Miskovic, J. Vukanic, T. E. Madey, *Surf. Sci.* **169**, 405 (1986).
20. R. Walkup and Ph. Avouris, *Phys. Rev. Lett.* **56**, 524 (1986).
21. A. L. Johnson, R. Stockbauer, D. Barak, T. E. Madey, in preparation.
22. H. Niehus, *Appl. Surf. Sci.* **13**, 292 (1982).
23. R. H. Stulen, *Springer Ser. Surf. Sci.* **4**, 130 (1985).
24. M. J. Dresser, M. D. Alvey, J. T. Yates, Jr., *Surf. Sci.* **169**, 91 (1986).
25. R. Jaeger *et al.*, *Phys. Rev. Lett.* **45**, 1870 (1980).
26. See, for example, *J. Vac. Sci. Technol. B* **1**, 947 (1983) and following pages.
27. P. Williams, *Springer Ser. Chem. Phys.* **24**, 184 (1983).
28. W. Riedl and D. Menzel, *Surf. Sci.* **163**, 39 (1985); M. D. Alvey, M. J. Dresser, J. T. Yates, Jr., *ibid.* **165**, 447 (1986).
29. F. P. Netzer and T. E. Madey, *Phys. Rev. Lett.* **47**, 928 (1981).
30. K. Bange, J. K. Sass, T. E. Madey, *Surf. Sci.* **162**, 252 (1985); in preparation.
31. K. Bange, J. K. Sass, T. E. Madey, *Surf. Sci.* **152/153**, 550 (1985); ———, E. Stuve, *ibid.*, in press.
32. Y. J. Chabal and S. B. Christman, *Phys. Rev. B* **29**, 6974 (1984); Y. J. Chabal, *ibid.*, p. 3677.
33. C. U. S. Larsson, A. L. Johnson, A. Flodström, T. E. Madey, in preparation.
34. W. Riedl and D. Menzel, *Springer Ser. Surf. Sci.* **4**, 136 (1985).
35. M. S. Isaacson, in *Principles and Techniques of Electron Microscopy*, M. A. Hayat, Ed. (Van Nostrand-Reinhold, New York, 1977), vol. 7, p. 1.
36. J. Fuggle and E. Umbach, in preparation.
37. R. Haglund and N. Tolk, *Springer Ser. Surf. Sci.* **4**, 277 (1985).

38. I thank my colleagues A. L. Johnson, C. U. S. Larsson, K. Bange, J. K. Sass, E. Stuve, D. E. Ramaker, R. Kurtz, and R. L. Stockbauer for their contributions to the work described herein; and A. L. Johnson, D. Barak, and R. Stockbauer for the computer graphics system used for Figs. 3 and 4. The PSD work at the National Bureau of Standards was supported in part by the Office of Naval Research; the ESDIAD work was supported in part by the Department of Energy, Division of Basic Energy Sciences.